Vol. 1 December, 1955 No. 5

# MINERALOGICAL JOURNAL

CONTENTS

High-temperature Optics of Natural Sodic Plagioclases ..... H. Kano...255
Clay Minerals of Decomposed Andesitic Agglomeratic Lava at Yoake ..... S. Aomine and T. Higashi...278
On the Electrical Conduction of Pyrite ..... A. Sasaki...290
The Number of Counts of Beta-Rays Detected by an End-Window Geiger-Mueller Counter (Part II) ..... N. Katayama...303
Dielectric Behaviour of Apophyllite and Analcite ..... R. Kiriyama, H. Ibamoto, M. Koizumi and R. Kitagaki...313

*Short Communications*

Boulangerite in Sulphide Ores from the Obira Mine, Kyushu, Japan ..... M. Miyahisa...323
A New Method for Estimating the Termination Effect in Fourier Analysis ..... K. Doi...329

**The Mineralogical Society of Japan**
Department of Geology and Mineralogy, Faculty of Science,
Hokkaido University, Sapporo, Japan

# MINERALOGICAL JOURNAL

published by

The Mineralogical Society of Japan



## EDITORIAL BOARD

Zyunpei HARADA, *Hokkaido University;* Teiichi ITO, *University of Tokyo;* (Chief) Nobuo KATAYAMA, *University of Tokyo;* Keiichi OMORI, *Tohoku University;* Ryôiti KIRIYAMA, *University of Osaka;* Seitaro TSUBOI, *University of Tokyo;* Takeo WATANABE, *University of Tokyo;* Toyofumi YOSHIMURA, *Kyushu University.*


### *Instructions to Contributors*

Manuscripts of articles should be submitted to the executive editor, Nobuo Katayama, at the College of General Education, University of Tokyo, Komaba, Meguro-ku, Tokyo. The manuscript should be type-written with double space lines, and not exceed 20 sheets of normal type-writing paper. References of literature should be in accordance with the forms used in the pages of this journal.

Plates and figures should be capable of reduction to not more than 10 by 15 centimetres. Line drawings should be in black India ink on white drawing board, tracing paper, or coordinate paper printed in blue. Photographs should be positive glossy prints.

Two referees chosen by the Editorial Board read the manuscript of article submitted before it is accepted for publication.

Thirty reprints without cover will be furnished to the author free of cost and without previous notice from him. Additional reprints will be furnished at cost when ordered.

The price of the journal to subscribers in Japan is 250 yen for a single copy (including postage), and to subscribers in other countries $ 1.00 (including postage).


*Printed in Japan*

MINERALOGICAL JOURNAL, VOL. 1, NO. 5, pp. 255-277, DECEMBER, 1955

# HIGH-TEMPERATURE OPTICS OF NATURAL SODIC PLAGIOCLASES

HIROSHI KANO

*Institute of Mining Geology, College of Mines, Akita University*

ABSTRACT

The author has recently discovered numerous examples of natural high-temperature plagioclases more sodic than An 35 from some Miocene rhyolite lavas in Japan. The optical properties of these high-temperature sodic plagioclases differ distinctly from those of what are regarded as low-temperature plagioclases and are similar to those of synthetic high-temperature albite reported by O. F. Tuttle and N. L. Bowen. In this paper, the author presents new data on the refractive indices, axial angles, extinction angles, and Köhler-angles of these high-temperature plagioclases, and revised stereograms showing migration of optical indicatrices and twinning-axes in them.

## *Introduction*

It has been generally accepted that plagioclases found in volcanic rocks differ optically from those found in plutonic or metamorphic rocks. The former are regarded to have been formed at high-temperatures, whereas the latter at low-temperatures.

Optical properties of high-temperature plagioclases, especially those of the compositions of An 35 to An 70, have been studied by some European authors such as A. Köhler[11)12)], H. Tertch[20)21)22)23)24)25)] and G. van der Kaaden[7)8)]. As to the high-temperature optics of albitic plagioclases more sodic than An 35, however, satisfactory information has not been provided by these authors. A. Köhler[13)] considered that difference between the high and low optics was small at the albitic end. Though Kaaden's elaborate measurements did not cover the range from An 26 to the albitic end, yet the properties of his most sodic material (An 27) showed marked difference from those

of the low-temperature plagioclase of the same composition[8]. Data on "anomalous" optics of some sodic plagioclases can be found in some previous literature. For examples, V. Sobolev[19] discovered a sodic plagioclase (An 25) with low 2Vx (52°-62°) from an alkalic dolerite in the traps of Ilimpeya River, Siberia. D.S. Beliankin[2] described an artificial albite with small 2Vx (31°-34°) and low refractive indices ($\gamma$ 1.533, $\alpha$ 1.525) from the crustal lining of a glass-furnace vault. He ascribed this "anomaly" not to the high content of $K_2O$, but to the particularly high temperature of its formation, as in the case of sanidine. E. Preuss[8] also reported a sodic oligoclase (An 11) with 2Vx 60° from a chondrite.

Recently, valuable contribution to the mineralogy of synthetic high-temprature albite and contiguous feldspars has been made by O.F. Tuttle and N.L. Bowen,[29] and F. Laves and U. Chaisson,[15] and the existence of the high- and low-temperature modifications of those plagioclases was confirmed. A sodic plagioclase (An 11) from a Tertiary obsidian of the San Juan region of Colorado, described by E.S. Larsen etc.[14] was found to belong to the high-temperature series as a result of the re-examination by Tuttle and Bowen.[29] However, available data on high-temperature optics of natural sodic plagioclases are not enough at present to complete determinative diagrams, especially the variation diagrams of Köhler-angles of which the high temperature series have been partly constructed from the data obtained by the previous authors for the plagioclases ranging from An 35 to An 70.

The author has fortunately obtained numerous materials of natural high-temperature plagioclases ranging from An 10 to An 35 from some rhyolite-lavas of the Miocene volcanic formation (so-called "Green-Tuff" formation) in northeastern Japan.

The present work was undertaken in the hope of supplying new data to the optics of plagioclase, and accomplishing their high temperature charts. The author intends also to revise and reconstruct Reinhardt's stereograms for the determination of the high-

temperature plagioclases, formerly presented by G. van der Kaaden.[8]

*Method of measurement*

Throughout the present work, anorthite-content of a plagioclase was determined solely by the refractive indices. The measurement was performed on a single crystal in a thin-section by the usual immersion method, using a Hilger's monochromatic light source.

Here, a procedure slightly modified from Bradley's "single crystal" method[3] was adopted. O. Bradley measured $\alpha'$- and $\gamma'$-index of a selected crystal showing maximum birefringence and then obtained the values for $\alpha$ and $\gamma$ by extrapolation, whereas the present author measured directly three principal indices $\alpha$, $\beta$ and $\gamma$ on any crystal in a thin section with the aid of a universal stage.

At first, thin section of rock was removed from its cover- and slide-glass, and the Canada balsam sticking on it was washed off by xylol and alkohol. After dried, the section was rested on the slide-glass and was immersed in a liquid with an appropriate index of refraction. Then, the section, now covered with cover-glass, was set on the universal stage. By the usual universal-stage manipulation, a plagioclase crystal in the section was brought into a fixed position so that the vibration directions of the faster and slower light waves should give any two of the three principal indices, and then the indices of the mineral were matched with those of the immersion liquid at a certain wave length with the monochromator.

Though the procedure needs considerable care and skill to keep the section from damage, this method has a great advantage: the three principal indices can critically be determined with far less number of manipulation than the customary method, and the errors introduced by the extrapolation as in the case of Bradley are eliminated; more important is that measurements can be repeated on the same crystal so that to eliminate the random errors accompanying measurement.

On determining the values of $\alpha_D$, $\beta_D$ and $\gamma_D$ from the observed

values of $\alpha$, $\beta$ and $\gamma$ for any wave length, Tsuboi's dispersion net[28] was used, regarding that difference between each dispersion of the three principal indices of the same crystal may be negligible.[27] Next, the An-content was determined by the determinative chart presented by F. Chayes[4]. As will be described later, $\gamma$-indices of many of the present materials with high-temperature optics deviate over the limits of error from the standard regression line for $\gamma$-index.

Probable errors in the procedure above described seem to be about $\pm 0.0005$ for refractive index measurement, and about $\pm 2\%$ for

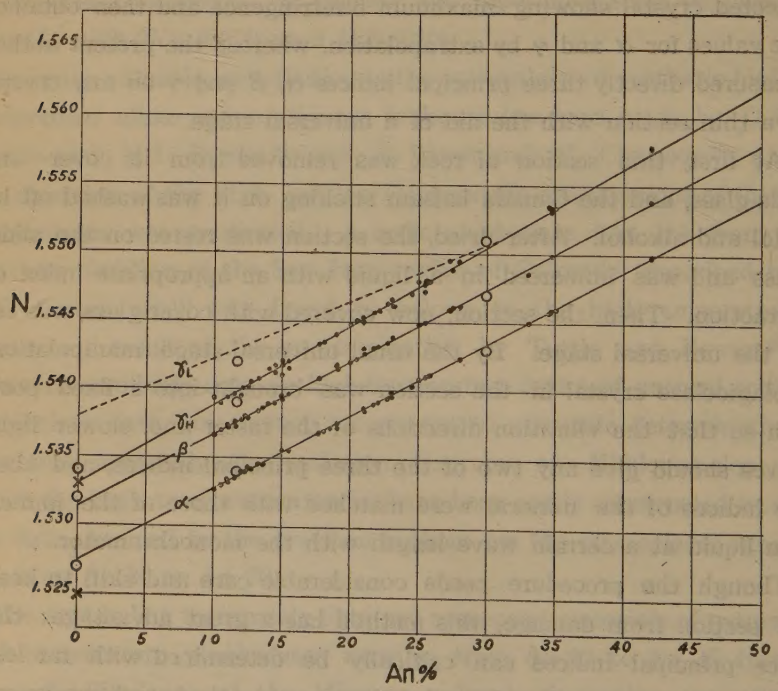


Fig. 1. Indices of refraction for sodic high-temperature plagioclases, plotted on the determinative chart after Chayes.[4]

- • Measured by the author.
- ○ An 30, natural, after Larsen.[14]
- ○ An 11½, natural, ditto.[14]
- ○ An 0, synthetic, after Tuttle and Bowen.[29]
- × An 0, synthetic, after Beliankin.[2]

An-content determination.

After the whole process of determination of the An-content was finished, axial angles, extinction angles and Köhler-angles were measured for the same crystal without changing the condition on the universal stage. In these cases, the measurements were made through D-light. For a zoned crystal, special care was taken to accomplish these measurements on a definite zone of the crystal.

Materials used in this investigation are all of sufficient size, 0.3 to 1.5 mm. in diameter, to permit detailed measurement. The results of measurement are shown in the Tables 1, 2, 3 and 4 according to the twinning laws, being arranged according to the increasing An-content.

### *Indices of refraction*

In Fig. 1, refractive indices of natural sodic plagioclases from An 10 to An 42 are projected on the determinative chart after F. Chayes[4]. Only the sodic half of the chart is shown in the figure and is modified a little as follows: the $\gamma$-line from An 30 to An 0 is composed of two divergent lines, $\gamma_L$ and $\gamma_H$ respectively, of which the former represents the $\gamma$-index regression of standard ('low') plagioclases, while the latter shows that of the high form as was suggested by F. Chayes[4].

It is a remarkable fact that most of the $\gamma$-values determined by the author lie not on the line $\gamma_L$, but on the line $\gamma_H$ within the limits of the error. It is also to be noticed, however, that the $\beta$- and $\alpha$-values of these high-temperature plagioclases are plotted along the $\beta$- and $\alpha$-line respectively, of the standard plagioclases without any appreciable deviation.

It may be concluded from this that all of the sodic plagioclases described here belong essentially to the typical high-temperature modifications. It is noteworthy, however, that the San Juan plagioclases (An 11½)[14] shows pronounced discrepancy.

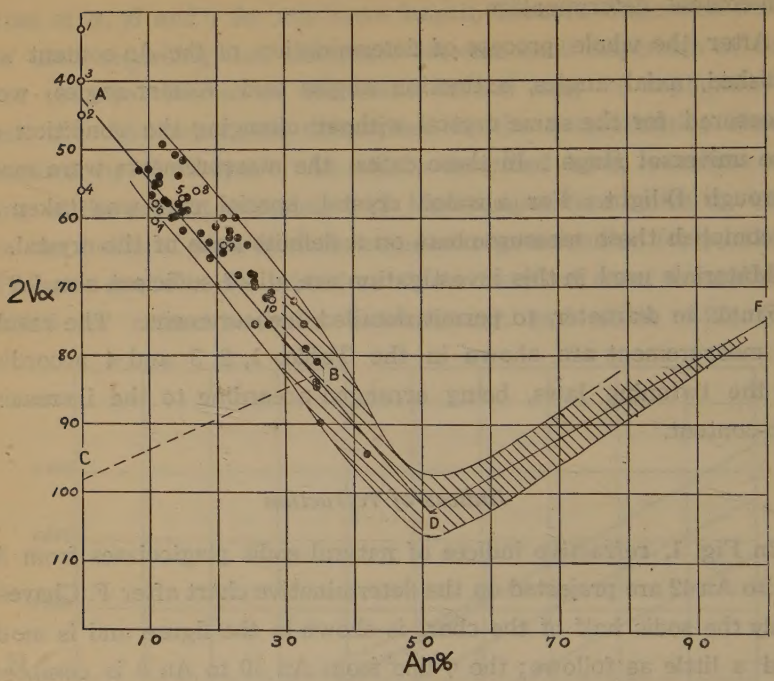


Fig. 2. Optic axial angles of sodic high-temperature plagioclases. • Measured by the author. The hatched zone represents the variation range of the axial angles of the intermediate and calcic plagioclases measured by Kaaden[8]. Open circles with numericals represent the previous data on high-temperature albites and contiguous plagioclases, as follows:
1, synthetic albite, after Beliankin,[2] 31°–34°;
2, synthetic albite, after Tuttle and Bowen[29], 45°;
3, heated natural albite, after Laves and Chaisson[15], 40°;
4, synthetic albite, ditto, 56° ± 3°;
5, An 15, natural, after Sobolev[19], 52°–62°;
6, An 11½, natural, after Tuttle and Bowen[29], 58°;
7, An 11, meteoritic, after Preuss[8], 60°½;
8, 9 and 10, heated natural, after Tuttle and Bowen[29].

### *Optic axial angles*

As reviewed above, the typical high-temperature plagioclases with albitic composition have without exception abnormally low values of

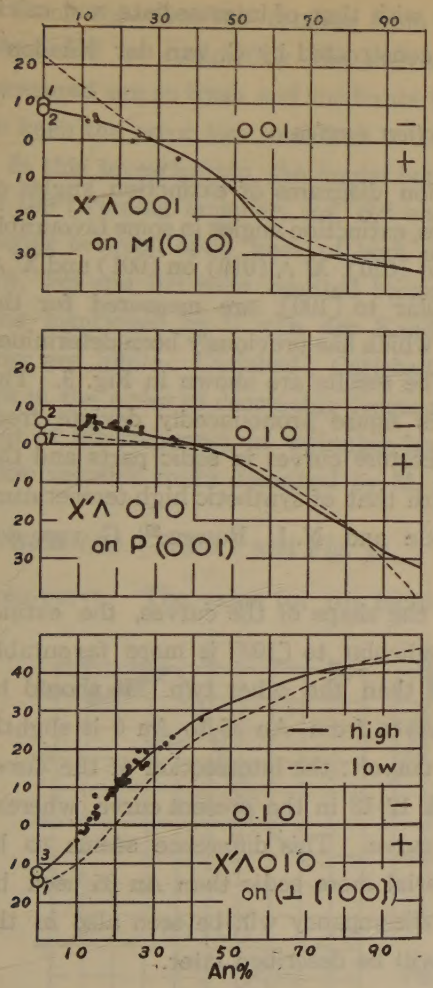


Fig. 3. Extinction angles on (010), (001) and the plane perpendicular to [100] for the sodic high-temperature plagioclases.

- Measured by the author.
- ○ 1, after Tuttle and Bowen[29].
- ○ 2, after Kaaden[8].
- ○ 3, after Beliankin[2].

axial angles comparing with those of the standard plagioclases. This can easily be inferred from the remarkable low values of $\gamma$-index described above, and consequently, the comparatively weak values of the partial birefringence ($\gamma$-$\beta$) of the high-temperature plagioclases under discussion.

As to the systematic relation between the axial angles and the composition of these plagioclases, it has been considered by O. F. Tuttle and N. L. Bowen[29] that 2Vx of high-temperature plagioclases more sodic than An 35 decreases straightly along the line BA in Fig. 2. The present investigation brings a similar result, but the scattering of projections is so large that the axial angle can not be used for the precise determination of the An-content. As shown in Fig. 2, every projection lies in a comparatively wide zone, about ±7° in width. It is worthy of attention that this zone is overlapped

in its calcic end (about An 40) with that of intermediate and calcic high-temperature plagioclases constructed by G. van der Kaaden[8].

### *Extinction angles*

To construct complete variation diagrams of extinction angles of the high-temperature plagioclases, extinction angles in some favourable directions such as X′ ∧ (001) on (010), X′ ∧ (010) on (001) and X′ ∧ (010) on the plane perpendicular to [100], are measured for the plagioclases, the composition of which has previously been determined from the refractive indices. The results are shown in Fig. 3. The high-temperature curves in this figure pronouncedly deviate from those of the relevant low-temperature curves in sodic parts and the terminal value coincides well with that of synthetic high-temperature albite presented by O. F. Tuttle and N. L. Bowen,[29] G. van der Kaaden[8] or D. S. Beliankin[2].

As may de easily seen from the shape of the curves, the extinction angle on the plane perpendicular to [100] is more favourable for the determinative purpose than the other two. It should be noted that the course of the curves from An 35 to An 0 is slightly different from that of Kaaden's curve[8]: the intersection of the curve with the (010)-trace lies near An 12–13 in the present curve, whereas it is about An 16 in Kaaden's curve. This difference seems to be mainly due to scarcity of material more sodic than An 35 used by G. van der Kaaden. A similar discrepancy will be seen also in the case of Köhler-angle curve as will be described later.

### *Köhler-angles*

It has generally been accepted that the Köhler-angle diagrams are most suited for the determination of An-content of plagioclase. Though several diagrams for the various twinning laws have been constructed, any reliable curve for the high-temperature modifications with the composition An 0 to An 35 have not been published as yet.

Using the materials ranging from An 10 to An 35, the author has succeeded in completing the curves in detail. All the crystals measured are so fresh and moderate in size, that it is not so difficult to keep the error less than 2°.

In this investigation, the angles between optic vectors of both sides of the twinning lamellae, $\alpha\alpha$, $\beta\beta$ and $\gamma\gamma$ were measured, while the angles between optic axes of both sides of the twinning lamellae, AA, BB and AB were omitted because of the variability of 2V as was mentioned by G. van der Kaaden[8]. The observed twinning laws are albite-, Carlsbad-, Carlsbad-albite- and pericline (acline)-law in the order of decreasing frequency. This order coincides with that of the frequency of twinning laws of plagioclases occurring in felsic volcanic rocks described by M. Gorai[5].

*Albite-law* (Table 1 and Fig. 4)

$\alpha\alpha$-curve. The value for $\alpha\alpha$ increases up to nearly 180° at An

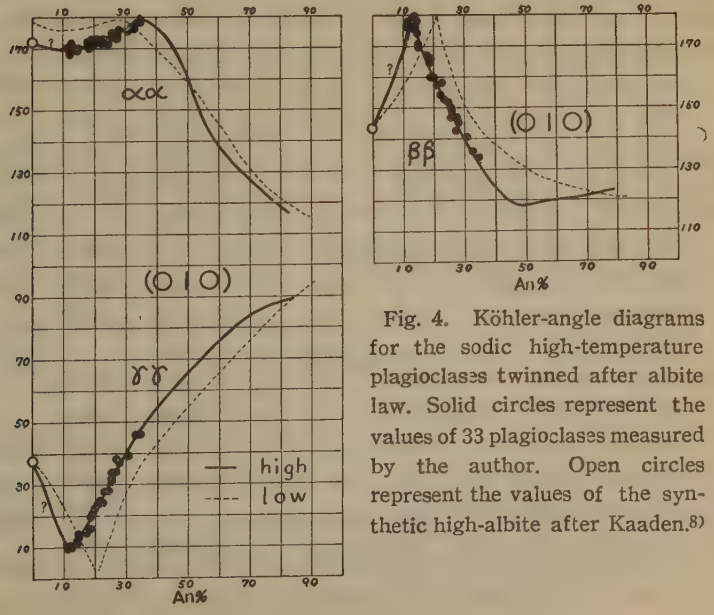


Fig. 4. Köhler-angle diagrams for the sodic high-temperature plagioclases twinned after albite law. Solid circles represent the values of 33 plagioclases measured by the author. Open circles represent the values of the synthetic high-albite after Kaaden.[8]

Table 1. Optical data of high-temperature sodic plagioclases twinned after albite law.

| No. | Locality | Köhler-angles αα | Köhler-angles ββ | Köhler-angles γγ | 2Vx | Extinction angles (⊥[100])(001) | Extinction angles (010) | | Refractive indices γ | Refractive indices β | Refractive indices α | An% |
|---|---|---|---|---|---|---|---|---|---|---|---|---|
| 1 | Kaitorima | 170½° | 176° | 9½° | 54° | | −5° | −5° | 1.5396 | 1.5372 | 1.5335 | 11½ |
| 2 | Oga, 81109 | 170 | 176½ | 11½ | 49½ | + 2° | −6 | | 1.5396 | 1.5378 | 1.5340 | 12 |
| 3 | 〃 | 168 | 178 | 12 | | | | −5½ | 1.5402 | 1.5380 | 1.5340 | 12¼ |
| 4 | 〃 | 170½ | 177½ | 11 | 57½ | 0 | −7¾ | | 1.5402 | 1.5379 | 1.5343 | 12½ |
| 5 | Kaitorima | 170½ | 176½ | 12 | 60 | − 1½ | −7½ | −5 | 1.5408 | 1.5384 | 1.5346 | 13¼ |
| 6 | Oga, 81109 | 170 | 176 | 11 | 51 | | −4 | | 1.5415 | 1.5388 | | 14 |
| 7 | 〃 | 169 | 180 | 11 | 59½ | − 3½ | −5½ | | 1.5417 | 1.5392 | 1.5350 | 14¼ |
| 8 | 〃 | 171 | 174½ | 9 | 60 | − 3½ | | | 1.5408 | 1.5390 | 1.5341 | 14½ |
| 9 | Kaitorima | 170 | 174 | 12 | 54 | − 3½ | | | 1.5412 | 1.5390 | | 14½ |
| 10 | Oga, 81109 | 170 | 178 | 9½ | 66 | − 5 | | | 1.5410 | 1.5390 | 1.5350 | 14½ |
| 11 | Kaitorima | 170 | 170½ | 14½ | 62 | − 5 | | | 1.5410 | 1.5392 | 1.5356 | 15 |
| 12 | 〃 | 170 | 169½ | 14 | 51½ | | | | 1.5418 | 1.5393 | | 15 |
| 13 | 〃 | 172 | 167 | 14 | | − 7 | −5 | | 1.5435 | | 1.5370 | 18 |
| 14 | 〃 | 170 | 165 | 20 | | − 8 | | | 1.5440 | | 1.5372 | 18½ |
| 15 | 〃 | 171 | 166 | 16 | 66 | − 8½ | −5½ | | 1.5441 | 1.5417 | 1.5375 | 19 |
| 16 | Oga, 81506 | 173 | 160 | 21 | 63½ | − 9½ | −4 | | 1.5442 | 1.5416 | 1.5368 | 19 |
| 17 | 〃 | 172 | 159½ | 22 | 61¼ | − 9½ | | | 1.5448 | 1.5420 | | 20 |
| 18 | 〃 | 173 | 157 | 24 | 60 | −12 | | | 1.5452 | 1.5426 | 1.5385 | 21 |
| 19 | 〃 | 172½ | 154 | 25 | 63 | | −4 | | 1.5458 | 1.5432 | 1.5390 | 21¾ |
| 20 | Oga, 81302 | 171½ | 158 | 24 | 60 | | | | 1.5463 | 1.5436 | 1.5394 | 22¾ |
| 21 | Oga, 81506 | 173 | 152½ | 28 | 68½ | −14 | | | 1.5467 | 1.5438 | 1.5396 | 23 |
| 22 | Oga, 81302 | 171 | 152 | 28 | 64 | | | | 1.5472 | | 1.5403 | 24½ |
| 23 | Oga, 81208 | 175 | 146½ | 34 | 68½ | −16½ | −3 | −2 | 1.5478 | 1.5449 | 1.5410 | 25½ |
| 24 | 〃 | 174 | 148 | 32 | 76 | | −3 | | 1.5480 | 1.5450 | 1.5410 | 25½ |
| 25 | Inausi | 174 | 149 | 31 | 70 | −16 | | | 1.5472 | 1.5450 | | 25½ |
| 26 | 〃 | 172 | 145½ | 35 | | | −4 | | 1.5480 | | 1.5412 | 25¾ |
| 27 | Oga, pebble | 174½ | 142½ | 38½ | 71¾ | −19½ | | | 1.5496 | 1.5460 | | 27½ |
| 28 | 〃 | 173 | 147 | 34 | 75½ | −15 | | | 1.5488 | 1.5461 | | 27 |
| 29 | Oga, 81302 | 176 | 145 | 37 | 71 | −16 | | | 1.5495 | 1.5462 | 1.5424 | 28 |
| 30 | 〃 | 175 | 140½ | 39 | 72 | −20 | | | 1.5516 | 1.5480 | 1.5442 | 31½ |
| 31 | Babanome | 176 | 136 | 45½ | 75½ | −21 | | | | 1.5486 | 1.5450 | 33 |
| 32 | Oga, 81503 | 178½ | 134 | 46 | 84¼ | −23½ | | | 1.5534 | 1.5499 | | 34 |

35, and then it decreases gradually to 170° near An 12–13. In the more albitic side than An 12–13, it may be considered that the curve will be raised slightly up to 172° at An 0 as may be indicated from the data of the synthetic high-temperature albite[8].

$\beta\beta$-curve. As may be inferred from the curve of the low-temperature plagioclases, the $\beta\beta$-value of the high-temperature plagioclase increases also up to 180° in the sodic side of the curve. Through the statistical observation, it may be concluded that the maximum value of $\beta\beta$ is attained at the composition of about An 13½.

It may be inferred from the extrapolation of Kaaden's data, however, that the curve will reach to the maximum point at the composition of about An 15–16. This deviation is apparently beyond the limits of observational error. For instance, G. van der Kaaden[8] describes 149°½, 149°, 138°, 134° and 133° as the $\beta\beta$-values for An 27, An 28, An 33, An 34 and An 35, respectively. According to the present diagram, however, these values correspond to An 25½, An 25, An 31, An 33 and An 34, respectively. As in the case of the extinction angle curve, such discrepancy seems to be due to the scarcity of data available to Kaaden on the more sodic plagioclases than An 27. The curve in the most sodic side may be supposed to decline with steep inclination from An 13½ down to An 0.

$\gamma\gamma$-curve. This curve shows a minimum in the vicinity of An 11–14, at which the angle of $\gamma\gamma$ decreases to about 10°, and then the curve is raised up in the more albitic side than An 11, until it terminates at An 0 ($\gamma\gamma$=38°). In this case also, the extension of Kaaden's curve in the sodic side deviates slightly toward the low-temperature curve from the present one.

*Carlsbad-law* (Table 2, Fig. 5 a)

The $\alpha\alpha$-value increases gradually at nearly equal rate from An 33 to An 10 and forms a comparatively smooth and gentle curve, whose extension may be directly connected with the high-temperature albite end (145°). On the contrary, $\beta\beta$-curve as well as $\gamma\gamma$ curve

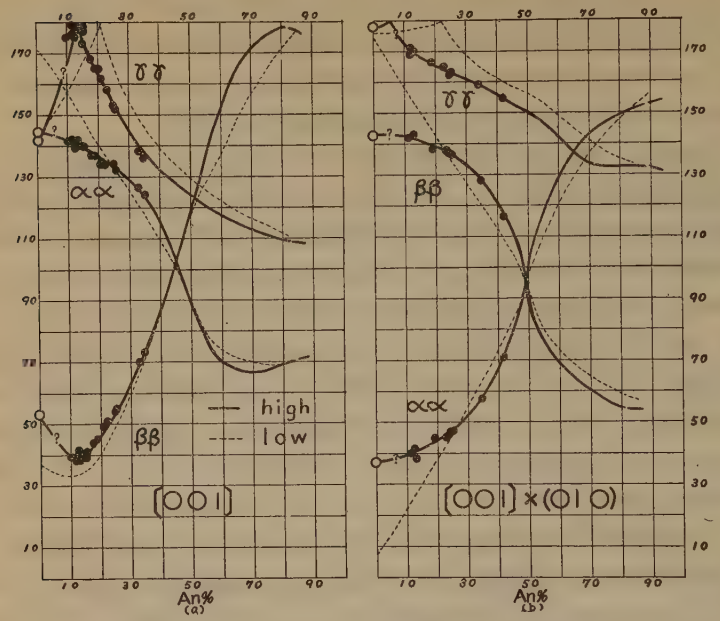


Fig. 5 a, b. Köhler-angle diagrams for the sodic high-temperature plagioclases twinned after (a) Carlsbad- and (b) Carlsbad-albite-law, respectively. Solid circles represent the author's data; open circles, values for the synthetic high-albite after Kaaden[8].

has a turning point at about An 13. There is no data filling the gap between An 10 and An 0, but the mode of the slight changes of $\beta\beta$- or $\gamma\gamma$-values from An 15 to An 10 indicates apparent turning of the curve.

*Carlsbad-albite-law* (Table 3, Fig. 5 b)

Though the number of measurements is small, in this case, each measurement is most accurate and reliable. It is apparent that the extension of the sodic end of the $\alpha\alpha$- or $\beta\beta$-curve may be directly connected with the albitic end. As to the $\gamma\gamma$-curve, however, there seems to be slight turning at some point between An 10 and An 0. These curves are most suitable for the determination of the high-

Table 2. Optical data of high-temperature sodic plagioclases twinned after Carlsbad law.

| No. | Locality | Köhler-angles | | | 2Vx | Extinction angles on | | | Refractive indices | | | An% |
|---|---|---|---|---|---|---|---|---|---|---|---|---|
| | | αα | ββ | γγ | | (⊥[100]) | (001) | (010) | γ | β | α | |
| 33 | Oga, 81109 | 141½° | 39½° | 175° | 53° | + 4° | −4° | | 1.5393 | 1.5367 | 1.5327 | 10 |
| 34 | 〃 | 141½ | 39 | 176 | 55 | + 2 | −5 | | 1.5397 | 1.5376 | 1.5335 | 11½ |
| 1* | Kaitorima | 142 | 38 | 179 | 54 | | −5 | −5° | 1.5396 | 1.5372 | 1.5335 | 11½ |
| 35 | 〃 | 139 | 40 | 178 | 57½ | + 1½ | | | 1.5402 | 1.5380 | —— | 12½ |
| 4* | Oga, 81109 | 139½ | 41½ | 175 | 57½ | ± 0 | −7¾ | | 1.5402 | 1.5379 | 1.5343 | 12½ |
| 6* | Kaitorima | 142 | 38 | 177½ | 60 | − 1½ | −7½ | −5 | 1.5408 | 1.5384 | 1.5346 | 13¼ |
| 36 | Oga, 81109 | 140 | 39 | 173 | 59 | ± 0 | −5½ | | 1.5422 | 1.5395 | —— | 15 |
| 37 | Kaitorima | 140 | 41 | 178½ | 59 | − 2½ | | | 1.5415 | 1.5396 | 1.5356 | 15½ |
| 38 | Oga, 81109 | 140 | 40 | 177 | 57 | − 1½ | | | 1.5420 | 1.5397 | 1.5355 | 15½ |
| 39 | Oga, 81506 | 137 | 44 | 168 | 62¼ | − 7 | | | 1.5434 | 1.5408 | 1.5369 | 17¾ |
| 16* | 〃 | 137 | 45 | 165 | 63½ | − 9½ | −4 | | 1.5442 | 1.5416 | 1.5368 | 19 |
| 40 | 〃 | 134 | 49 | 165 | | −12 | −4 | | 1.5452 | 1.5423 | —— | 20½ |
| 41 | 〃 | 135 | 49 | 162 | 65 | −11 | | | 1.5453 | 1.5430 | 1.5387 | 21 |
| 42 | 〃 | 134 | 51 | 157 | 62 | −13 | | | 1.5458 | 1.5432 | 1.5392 | 22 |
| 43 | Oga, pebble | 134 | 54 | 153 | 68¼ | −17 | | | 1.5480 | 1.5448 | 1.5408 | 25 |
| 23* | Oga, 81208 | 132 | 55 | 151¾ | 68½ | −16½ | −3 | −2 | 1.5478 | 1.5449 | 1.5410 | 25½ |
| 44 | Babanome | 126½ | 70 | 138 | 79 | −21½ | | | —— | 1.5486 | 1.5450 | 33 |
| 45 | 〃 | 124 | 74 | 136 | 81 | | | | 1.5532 | 1.5500 | 1.5460 | 34¾ |

* The same crystal as in Table 1.

Table 3. Optical data of high-temperature sodic plagioclases twinned after Calrsbad-albite law.

| No. | Locality | Köhler-angles | | | 2Vx | Extinction angles on | | | Refractive indices | | | An% |
|---|---|---|---|---|---|---|---|---|---|---|---|---|
| | | αα | ββ | γγ | | (⊥[100]) | (001) | (010) | γ | β | α | |
| 1* | Kaitorima | 40° | 142° | 169° | 54° | | −5° | −5° | 1.5396 | 1.5372 | 1.5335 | 11½ |
| 4* | Oga, 81109 | 41½ | 139 | 171 | 57½ | ± 0° | −7¾ | | 1.5402 | 1.5379 | 1.5343 | 12½ |
| 5* | Kaitorima | 38 | 143 | 170 | 60 | − 1½ | −7½ | −5 | 1.5408 | 1.5384 | 1.5346 | 13¼ |
| 16* | Oga, 81506 | 45 | 138 | 166½ | 63½ | − 9½ | −4 | | 1.5442 | 1.5416 | 1.5368 | 19 |
| 46 | Babanome | 45 | 137½ | 165 | 68½ | −11¼ | −6 | | 1.5455 | 1.5430 | 1.5390 | 23 |
| 22* | Oga, 81302 | 47 | 137 | 162 | 64 | | | | 1.5472 | —— | 1.5403 | 24½ |
| 23* | Oga, 81208 | 47 | 136½ | 163 | 68½ | −16½ | −3 | −2 | 1.5478 | 1.5449 | 1.5410 | 25½ |
| 47 | Oga, 81109 | 57½ | 128 | 159 | 84 | | −2 | | 1.5535 | —— | 1.5458 | 34½ |
| 48 | Oga, 81208 | 70½ | 116 | 154½ | 94½ | −27¾ | | | 1.5578 | 1.5538 | 1.5498 | 42 |

No. 46: lath-shaped crystal in groundmass.

No. 47: calcic core of No. 33.

No. 48: calcic core of No. 23.

* The same crystal as in Table 1.

temperature oligoclase.

Table 4. Optical data of high-temperature sodic plagioclases twinned after pericline (acline)-law.

| No. | Locality | Köhler-angles | | | 2Vx | Extinction angles on | | Refractive indices | | | An% |
|---|---|---|---|---|---|---|---|---|---|---|---|
| | | αα | ββ | γγ | | (⊥[100]) (001) | (010) | γ | β | α | |
| 49 | Oga, 81109 | 167° | 167° | 18° | 55° | | | —— | 1.5373 | 1.5333 | 11 |
| 50 | 〃 | 171½ | 178½ | 9 | 60 | | −6¼° | —— | 1.5386 | 1.5345 | 13½ |
| 51 | Kaitorima | 169 | 171 | 15½ | 58 | − 8° | | 1.5418 | 1.5390 | —— | 14½ |
| 11* | 〃 | 172 | 166 | 16 | 62 | − 5 | | 1.5410 | 1.5392 | 1.5356 | 15 |
| 52 | Oga, 81506 | 172 | 152 | 30 | 64 | −11 | | 1.5450 | 1.5426 | —— | 21 |
| 53 | 〃 | 172 | 143½ | 37 | 63 | −15½ | ±0 | 1.5462 | 1.5438 | 1.5398 | 23 |
| 54 | Oga, 80704 | 174 | 139½ | 41 | 69½ | −19½ | | 1.5478 | 1.5450 | —— | 25½ |
| 55 | Babanome | 180 | 125 | 55 | 90 | | −2° −5½ | 1.5535 | —— | 1.5460 | 35 |

* The same crystal as in Table 1.

*Pericline (acline)-law* (Table 4)

On account of the comparatively rare occurrence of this twin, the diagram was not constructed. It may be considered, however, that the Köhler-angle curve for this twinning law follows a similar course as that of the curve for the albite twin.

### *Revision of the Reinhardt's stereograms for the high-temperature plagioclases*

Reinhardt's stereograms which have been extensively used for the determination of the An-content as well as the twinning laws of plagioclases were compiled for the whole series of the high-temperature plagioclases by G. van der Kaaden[8]. and I. D. Muir [16]. As for the migration curves from An 35½ to An 0, however, owing to the scarcity of data then available their interpolation seems somewhat ambiguous, as may be easily inferred from

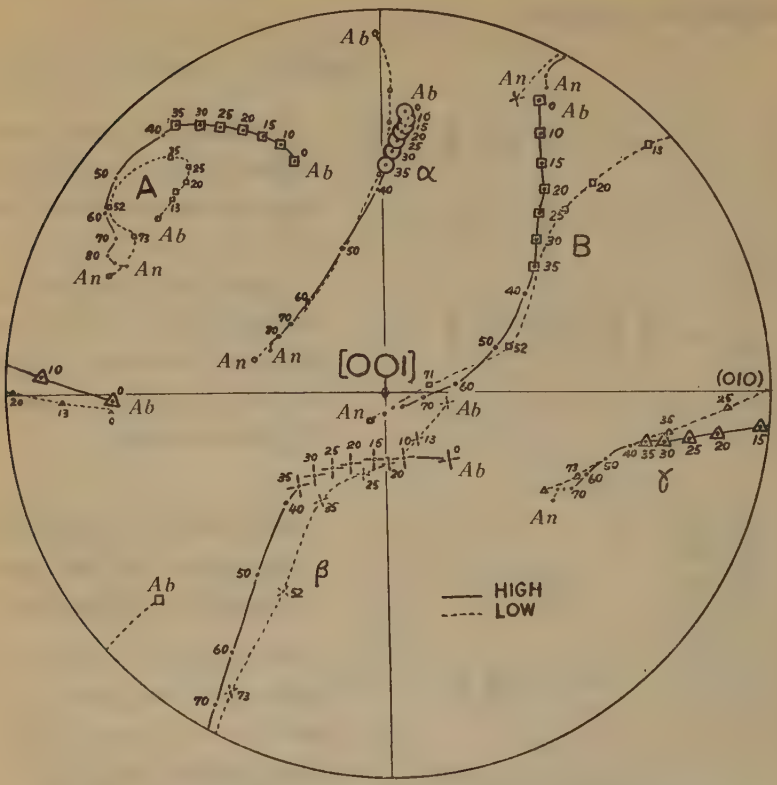


Fig. 6. Stereogram I, showing migration-curves of the optic indicatrices, α, β, and γ, and the optic axes, A and B, of sodic high-temperature plagioclases, projected perpendidular to c-axis [001]. Curves for the contiguous high temperature plagioclase series and the low-temperature plagioclase series are drawn after Kaaden's Stereogram I.[8)]

the above mentioned deviation of Kaaden's data on Köhler angles from those of the author. On applying the actually observed data to the stereogram of Kaaden, the position of (010)-pole is correlated to somewhat higher An-content than what is carefully determined from the refractive indices by the present author. The sodic parts of the migration curves of Kaaden and Muir particularly of (010)- and [010]-poles, therefore, should be revised.

Table 5. Constructional data for Stereogram I (Fig. 6).

| An % | | 0* | 10 | 15 | 20 | 25 | 30 | 35 |
|---|---|---|---|---|---|---|---|---|
| Köhler-angles for albite law | αα | 172° | 170° | 171° | 172° | 174° | 176° | 180° |
| | ββ | 143½ | 170 | 173 | 160 | 149 | 140 | 132 |
| | γγ | 38 | 13 | 13 | 22 | 31 | 40 | 47½ |
| [⊥(010)] ∧ α | | 86° | 85° | 85½° | 86° | 87° | 88° | 90° |
| [⊥(010)] ∧ β | | 71¾ | 85 | 86½ | 80 | 74½ | 70 | 66 |
| [⊥(010)] ∧ γ | | 19 | 6½ | 6½ | 11 | 15½ | 20 | 23¼ |
| Köhler-angles for Carlsbad law | αα | 145° | 142° | 140° | 137° | 133° | 129° | 124° |
| | ββ | 53 | 40 | 40 | 46 | 54½ | 63½ | 73 |
| | γγ | 142 | 168 | 176 | 164 | 154 | 145 | 138 |
| [001] ∧ α | | 72½° | 71° | 70° | 68½° | 66½° | 64½° | 62° |
| [001] ∧ β | | 26½ | 20 | 20 | 23 | 27¼ | 31¾ | 36½ |
| [001] ∧ γ | | 71 | 84 | 88 | 82 | 77 | 72½ | 69 |
| Köhler-angles for Carlsbad-albite law | αα | 37° | 39½° | 41½° | 44° | 47½° | 52° | 56° |
| | ββ | 142½ | 142 | 140½ | 138½ | 136½ | 132½ | 130 |
| | γγ | 178 | 174 | 168½ | 165 | 163 | 161 | 158 |
| [⊥[001] in (010)] ∧ α | | 18½° | 19¾° | 20¾° | 22° | 23¾° | 26° | 28° |
| [⊥[001] in (010)] ∧ β | | 71¼ | 71 | 70¼ | 69¼ | 68¼ | 66¼ | 65 |
| [⊥[001] in (010)] ∧ γ | | 89 | 87 | 84¼ | 82½ | 81½ | 80½ | 79 |
| 2Vx (average) | | 50° | 52° | 57° | 63° | 69° | 76° | 84° |

* after G. van der Kaaden[8].

Stereogram I (Fig. 6). In this stereogram the migration curves of optical vectors are constructed with regard to c-axis [001].

According to the author's data (Table 5), the revised positions of An 10, An 15, An 20, An 25, An 30 and An 35 are plotted on the curves of $\alpha$, $\beta$, $\gamma$, A and B. Compared with the stereograms of Kaaden and Muir, it is noted that $\gamma$ takes a considerably different course, especially in the sodic part. As to the other vectors, however, there is no essential differences between the two kinds of diagrams.

Stereogam II (Fig. 7) shows the projection of the poles of (010).

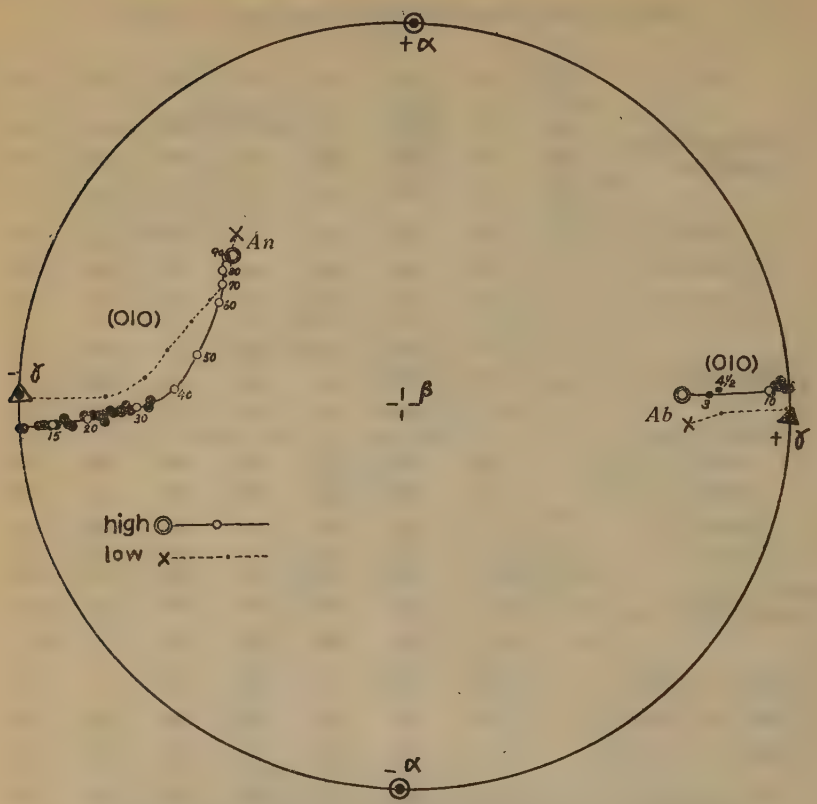


Fig. 7. Stereogram II, showing the migration curve of the (010)-poles for sodic high-temperature plagioclases, projected perpendicular to β. Curves for the contiguous high-temperature series and the low-series are drawn after Kaaden's Stereogram II.[8)]

Though the migrating course is almost similar to those in Kaaden's and Muir's stereogram, the positions of poles corresponding to An 10 and An 20 are shifted farther to the left (albitic) side. The angle $\beta\beta$ reduces to zero at the intersection of the curve with the ground circle of the stereogram, and the composition of this point is about An $13\frac{1}{2}$.

In Stereogram III (Fig. 8) poles of [001], [⊥[001] in (010)], and [010] are projected as the symmetry axes of Carlsbad-, Carlsbad-albite- and pericline (acline)- twins. In this stereogram, also, the

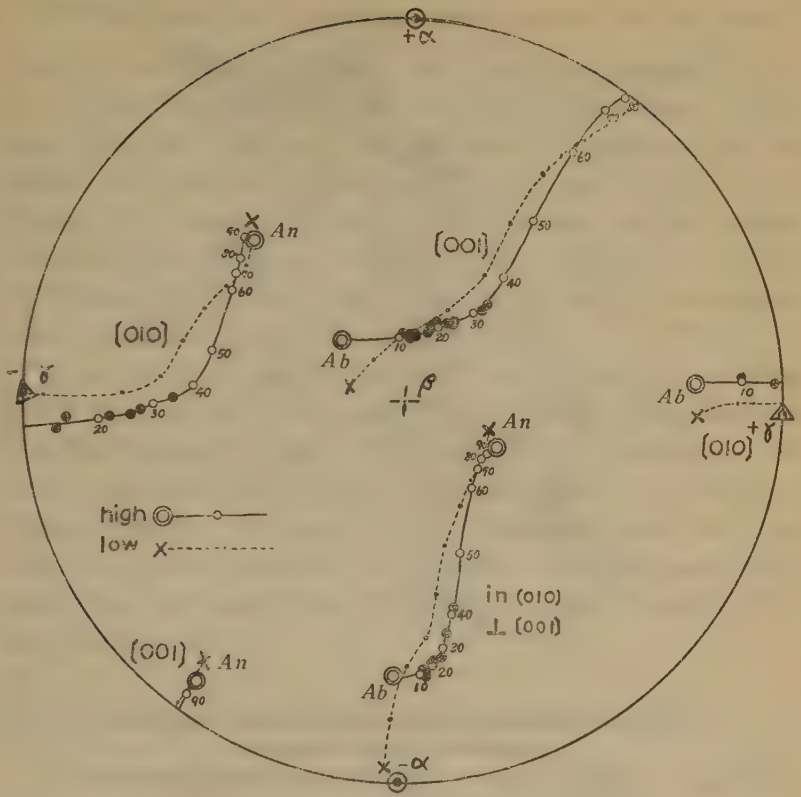


Fig. 8. Stereogram III, showing migration-curves of the poles of [001], ⊥[001] in (010) and [010], respectively, projected perpendicular to β. Curves for the contiguous high-temperature plagioclase series and the low-series are drawn after Kaaden's Stereogram III.[8]

positions of An 10, An 20 and An 30 on the [001]-migration curve deviate considerably from those in Kaaden's stereogram and are shifted slightly to the right (calcic) side as a necessary result of the deviation of the γγ-curve mentioned above. As to the poles of [⊥[001] in (010)], however, there seems to be no significant difference from what are given by Kaaden.

Fig. 9. Distribution of the anorthoclase-high-temperature oligoclase rhyolites in Japan.

1, Sinzan, Oga-peninsula, Akita Prefecture (No.81109).[9]
2, Kaitorima, Hokkaido.[17]
3, Hutomiyama, Toyama Prefecture.[6]
4, Higasi-Kuttian Mine, Hokkaido.[17]
5, Kayanuma Coal-mine Hokkaido.[17]
6, Nisi-Simamaki, Hokkaido.[17]
7, Asano Coal-mine, Hokkaido.[17]
8, Inausi Mine, Hokkaido.[10]
9, Oizumi, Yamagata Prefecture.[9]
10, Iwamisannai, Akita Prefecture.*
11, Sakaigawa, Toyama Prefecture.**

The dotted area represents the distribution of the so-called "Green-Tuff' formation.

* Recently discovered by the author.

** Communicated from T. Matsumoto, Osaka Municipal University.

*Brief notes on the geology and petrography of the host rocks*

Most of the sodic plagioclases with typical high-temperature optics just described are commonly found as idiomorphic phenocrysts in some rhyolites, which have been considered to represent the final products of extensive volcanic activities of calc-alkalic type in Miocene. It is quite likely that their distribution may be confined to definite parts, in time as well as in space, of the so-called "Green-Tuff" region in northern part of Honsyu and also in southwestern as well as northeastern Hokkaido (Fig. 9).

The present author and T. Takayasu[9] have provided some convincing evidences on the age of some of the rhyolites petrographically as well as stratigraphically. According to their conclusion, it has been believed that most of the rocks were erupted at the later stage of lower Miocene. Moreover, it is of genetic significance that occurrence of rhyolites including such extremely sodic high-temperature plagioclases has never been reported from the recent volcanic provinces in Japan.

Table 6. Modal composition of the anorthoclase-high-oligoclase-rhyolites (vol.%)

| | | Oga (No. 81109) | Kaitorima, Hokkaido | Inausi,* Hokkaido |
|---|---|---|---|---|
| High-oligoclase | phenocrysts | 5.9 (An 12) | 6.6 (An 14) | 8.4 (An25)** |
| Anorthoclase | phenocrysts | 0.9 (Or 40) | 4.0 (Or 50) | 2.9 (Or75)** |
| Quartz | phenocrysts | 0.6 | 0.1 | 7.7 |
| Biotite | phenocrysts | 0.9 | 0.1 | 4.1 |
| Opaque minerals | phenocrysts | 1.5 | 2.2 | 1.1 |
| Anorthoclase | groundmass | 67.2 (Or 35) | | |
| Quartz | groundmass | 23.0 | 87.0 | 75.8 |
| Others | groundmass | 0.0 | | |
| | | 100.0 | 100.0 | 100.0 |
| Or: Ab: An | | 33: 66: 1 | | 37: 48: 15 |

* Chemically analysed by Y. Katsui.[10] ** Measured by the author.

One of the most characteristic features of these rhyolites is the sparing but persistent presence of distinct anorthoclase-phenocrysts, particularly in the most felsic differentiates such as those from Sinzan of Oga-peninsula (No. 81109), Kaitorima and Inausi of Hokkaido. Modal compositions of these rocks are shown in Table 6.

As has been observed by some previous authors,[1)14)25)] as the An -content of plagioclase decreases, the Ab-content of accompanying anorthoclase increases. In this connection, it is worthy of attention that the most sodic plagioclase found in alkali-rhyolites with abundant anorthoclase (Or 55) described by T. Tomita[25)] from the Dogo Island of Oki in the Circum-Japan-Sea alkalic rock province is not less than 30 per cent in An-content according to the author's measurement, whereas in the calc-alkalic rhyolites accompanying anorthoclase under discussion there are as sodic plagioclases as An 10.

*Acknowledgements*

The author wishes to express his sincere thanks to Dr. Toshio Ishikawa, Hokkaido University, for many helps and valuable suggestions, and to Dr. Kenzo Yagi, Tohoku University, for critical reading the manuscript. He is also indebted to Mr. Taisuke Takayasu, Akita University, Dr. Tadahiro Nemoto, Geological Survey of Japan, Mr. Hokuitiro Omati, Hokkaido University, Dr. Yoshinori Kawano, Geological Survey of Japan, and Dr. Keinosuke Tan, Akita University for providing him numerous materials used in this investigation, and to Messrs. Hukutaro Hori, Tokyo University, Kazuo Miyagi and Katutosi Uruno, Tohoku University, for some of the literature cited here.

This investigation has been financially supported in part by a Grant from the Expenditure for Scientific Research from the Ministry of Education, which is greatly appreciated.

## References

1) Barth, T. F. W.: Die Entstehung der Gesteine, Berlin (1939).

2) Beliankin, D. S.: Compt. Rend. Ac. Sc. U. R. S. S., 3, 651, cited from Min. Abstr.,6, 294, (1935).
3) Bradley, O.: Min. Mag., 30, 227 (1953).
4) Chayes F.: Am. J. Sci., BOWEN-Volume, 85 (1952).
5) Gorai, M.: Am. Mineral., 36, 884 (1951).
6) Imamura, S.: J. Geol. Soc. Japan, 39, 669 (1932). (in Japanese)
7) van der Kaaden, G.: Tschermaks Min. Petr. Mitt. I, Neue Folge, 295 (1949).
8) ——: Diss. Univ. Utrecht (1951).
9) Kano, H. and T. Takayasu: Rep. Research Inst. Underground Resources, Akita Univ., No. 13, 7 (1955). (in Japanese)
10) Katsui, Y.: Bull. Geol. Commit. of Hokkaido, 28, 25 (1955) (in Japanese)
11) Köhler, A.: Tschermaks Min. Petr. Mitt., 53. 24 (1941).
12) ——: Neues Jahrb. Min., Abt. A., 280 (1944),
13) ——: J. Geol., 57, 592 (1949).
14) Larsen, E. S., J. Irving, F. A. Gonyer and E. S. Larsen 3rd: Am. Mineral., 23, 227 (1938).
15) Laves, F and U. Chaisson: J. Geol., 58, 584 (1950).
16) Muir, I. D.: Min. Mag., 30, 545 (1955).
17) Nemoto, T.: J. Geol. Soc. Japan, 43, 396 (1937). (in Japanese)
18) Shibata, H.: J. Geol. Soc. Japan, 39, 669 (1932). (in Japanese)
19) Sobolev, V.: Mem. Soc. Russ. Min., Ser. 2, 62, 421 (1933), cited from Min. Abstr., 6, 293.
20) Tertsch, H.: Tschermaks Min. Petr. Mitt., 53, 50 (1941).
21) ——: Tschermaks Min., Petr. Mitt., 54, 193 (1942).
22) ——: Zentralblatte Min., Abt. A, 193 (1942).
23) ——: Ak. b. Wiss., 1 (1943).
24) ——: Neues Jahrb. Min., Abt. A, 274 (1944).
25) ——: Neues Jahrb. Min., 121 (1950).
26) Tomita, T.: J. Geol. Soc. Japan, 35, 463, 519 (1928). (in Japanese)
27) Tsuboi, S.: Min. Mag., 20, 93 (1923).
28) ——: Jap. J. Geol. Geogr., 11, 325 (1934).
29) Tuttle, O. F. and N. L. Bowen: J. Geol., 58, 572 (1950).

*Manuscript received June 22, 1955.*

Mineralogical Journal, Vol. 1, No. 5, pp. 278-289, December, 1955

# CLAY MINERALS OF DECOMPOSED ANDESITIC AGGLOMERATIC LAVA AT YOAKE*

Shigenori Aomine and Toshio Higashi

*Institute of Soil Science, Faculty of Agriculture, Kyushu University*

Abstract

Alluvial soils of the Chikugo River contain predominant montmorin in the clay fraction, being different with general alluvial soils in Kyushu. It is safely concluded that at least a part of that monmorin has been derived from the weathering products of the so-called Tsukushi lavas, especially agglomerate in the upper stream of the Chikugo River. The montmorin is poor in magnesium and iron, rich in aluminium, and high in exchange capacity of cation, retention of ethylene glycol, and fixation capacity of ammonium ions. It seems to belong to aluminian montmorillonite such as beidellite.

## *Introduction*

In a previous communication[3] by the present authors, they reported that the alluvial soils of the Chikugo River contained montmorin in their clay fractions, being different with the alluvial soils of the River Shira. The montmorin in the former soils was suggested to have been derived from the upper reaches of the Chikugo River. The basin of the River and its tributaries consists largely of volcanic rocks; various andesites, agglomerates, tuffs, pumices, and ashes, and these rocks have been classified by T. Akagi[1] into four groups of which the Tsukushi lavas are the oldest. Therefore, it is expected that montmorin is contained in weathering products from some of these rocks.

In this paper were reported some results of studies on clay

* Read at the meeting of the Science of Soil and Manure, Japan on April 4, 1955.

minerals in weathering products in the basin of the Chikugo River.

## *Materials and methods*

Samples were taken from outcrops of an andesite and two agglomerates at the river side of the Chikugo River about 100 m. down stream from the Yoake* Dam near the boundary of Oita and Fukuoka prefectures. The rocks belong to the Tsukushi lava which is the oldest type in this district.[1] They seem to be considerably subject to weathering, for they are so soft that one is able to dig them with a shovel. Samples used for this study are as follows.

No. 1: A light yellowish brown, sticky material occured in fissures between andesite blocks. When it is dried in air, it will be divided by many small fissures owing to marked shrinkage.

No. 2: A weathered material of an andesite, with remaining texture of the original rock and some crystals of feldspar and pyroxene. In general purplish brown, but mottled with light yellowish brown and light grey spots.

No. 6: A weathered agglomerate. Almost all the crystals in it are weathered into white, light yellow, light brown, dark brown, or blackish materials, but a few particles of pyroxene and feldspar are found both in rock fragments and matrices.

No. 7: White fragments in No. 6, thoroughly altered into clay minerals. The original rock is indeterminable. The fragments are found in comparatively limited parts together with those of two pyroxene andesite.

The samples for identification of clay minerals were prepared in two ways; one was bulk materials ground by an agate pestle in an agate mortar, and the other was clay fractions which were obtained as follows: particles with diameter less than 2 $\mu$. were separated, by means of a sedimentation method as usually applied in mechanical analysis of soils, from the material which had been kneaded in water with an agate pestle and dispersed for several hours on a rotatory shaker and clay suspensions thus obtained were flocculated with $CaCl_2$, and the clays were washed several times with a n-$CaCl_2$ solution in a centrifugal tube, then with methanol

* 夜明

until its supernatant liquid became free from chloride, dried in a room, and kept in a desiccator containing 50 per cent $H_2SO_4$.

Experimental methods used for identification of clay minerals were the same as in a previous work by one of the present authors[3]. Besides those, ammonium fixation capacity was determined in both wet and dry conditions. The samples were saturated with ammonium ions being treated with n-$NH_4Cl$ in a centrifugal tube three times, then they were washed with n-NaCl till leachate became free from ammonium ions. Fixed ammonium ions were determined by Kjeldahl method. Fixation in dry condition was carried out in the same way as in the wet condition, except that the samples were dried thrice with n-$NH_4Cl$ on a steam bath.

### *X-ray analysis*

X-ray diffraction patterns were photographed of the clay fractions of each sample variously treated, such as heated at 100, 400, 450, 500, and 600°C., or saturated with ethylene glycol or potassium ions. Table 1 shows the data obtained for samples treated with ethylene glycol.

Table 1 indicates that the samples can be classified into two groups; the one No. 1 and No. 6 with a strong line at 17.0 Å, and the other No. 2 and No. 7 with a strong line at 10.8 Å. Besides these lines, members of each group show several lines similar to the relevant lines of the same group both in intensity and in spacing with minor exceptions. This fact reveals that the sample No. 1 is composed of the same minerals as No. 6, and No. 2 the same as No. 7 respectively.

The line at 17.0 Å of the first group turns to about 16 Å by heating at 100°C. for 3 hours, to about 10 Å by heating at 400°C. or drying with n-KCl on a steam bath. This line is undoubtedly attributed to a basal spacing of montmorin. In the samples of the first group saturated with ethylene glycol, the diffraction patterns

Table 1. X-ray diffraction data of clay fractions (<2μ) saturated with ethylene glycol.

| No. 1 | | No. 2 | | No. 6 | | No. 7 | |
|---|---|---|---|---|---|---|---|
| *d*(Å) | *I* | *d*(Å) | *I* | *d*(Å) | *I* | *d*(Å) | *I* |
| 17.0 | I | | | 17.0 | II | | |
| 10.6 | IV | 10.8 | I | 10.6 | II | 10.8 | I |
| 7.2 | V | 7.3 | VI | | | 7.4 | IV |
| 5.60 | VI | | | | | | |
| (4.40 | II | 4.45 | II | 4.48 | II | (4.45 | II |
| (4.04 | IV | 4.07 | III | 4.05 | III | (4.01 | IV |
| 3.58 | V | 3.62 | III | 3.62 | IV | 3.62 | III |
| 3.34 | VI | | | | | | |
| | | 3.21 | VI | | | | |
| 2.56 | III | (2.53 | IV | (2.57 | IV | 2.52 | IV |
| 2.35 | VI | 2.36 | V | 2.36 | VI | 2.35 | IV |
| 2.21 | VI | 2.22 | VI | 2.22 | V | 2.22 | V |
| 1.69 | IV | 1.68 | VI | 1.69 | VI | 1.68 | V |
| | | | | | | 1.65 | V |
| 1.50 | VI | 1.49 | III | 1.49 | IV | 1.49 | III |
| 1.32 | VI | | | | | | |
| | | 1.29 | VI | 1.29 | VI | 1.29 | V |
| 1.24 | VI | 1.24 | VI | 1.24 | VI | 1.24 | V |

*I*: intensity, I: very strong, II: strong, III: medium, IV: weak, V: very weak, VI: barely visible, (: reflection broadened.

have a very weak or no line at 7.2 Å which develops into a strong or weak one by heating at 100°C. for 3 hours, and disappears when temperature is raised to 450°C. or higher for 30 minutes. From these experiments, it is obvious that the samples contain more or less hydrated halloysite.

The second group is recognized to have hydrated halloysite, because the line at 10.8 Å observed in the samples treated with ethylene glycol disappears by heating at 100°C. and at the same time a line at 7.4 Å increases appreciably in intensity.

According to these results, it may be concluded as follows: The clay fraction of No. 1 contains predominant montmorin with hydrated halloysite and halloysite, that of No. 2 and 7 much hydrated halloysite with halloysite, and that of No. 6 consists of predominant montmorin in addition to hydrated holloysite.

### *Differential thermal analysis*

Differential thermograms of the clay fractions are given in Fig. 1. The fractions were treated in air above 50 per cent $H_2SO_4$ for several weeks to regulate hygroscopicity prior to the analysis.

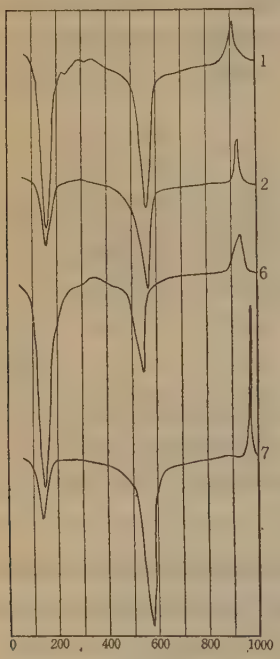


Fig. 1. Differential thermal analysis curves of the clay fractions (<2μ).

Every curve has two remarkable endothermic peaks at approximately 150 and 560°C. and one exothermic peak between 900 and 980°C.. The amplitude of the first endothermic peak is larger than that of the second peak for samples No. 1 and 6, the first group in X-ray analysis, while it is reversed for samples No. 2 and 7, the second group. There are further some differences between the two groups. The curves of the first group are uneven between the two endothermic peaks due to several minor thermal reactions; the first endothermic reaction, evaporation of hygroscopic water, does not finish sharply in the samples of the first group; the temperature of the second endothermic peak of the first group is slightly lower than that of the second group, and their exothermic reaction begins at 840 to 870°C., whereas the reaction of the second group does at 900°C. or higher, with a peak sharper than the former.

The curves of the second group resemble very much in shape those of hydrated halloysite partially dehydrated by 50 per cent $H_2SO_4$. This is in full agreement with the results obtained in the X-ray analysis indicating a majority of hydrated halloysite.

The curves of the first group suggest greater amount of hygroscopic water than any crystalline clay mineral indicates. They also indicate that the dehydration continues tardily up to higher than 200°C.. Sudo and Ossaka[12] reported that the temperatures of the three peaks of hydrated halloysite shifted with addition of allophane; the first endothermic and the exothermic peaks removed to lower temperature, and on the contrary the second peak removed to higher temperature. Similar relationship is seen in the curves of the second group in comparison with those of the first group. It seems that the clay fractions of the first group contain considerable amount of allophane in addition to hydrated halloysite. Judging from the X-ray diffraction patterns montmorin is present in those clay fractions, but any evidence supporting was not recognized in the thermograms of this group.

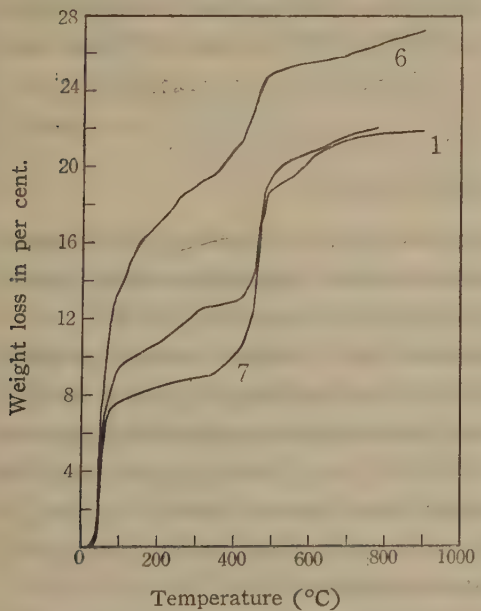

Fig. 2. Dehydration curves of the clay fractions (<2μ).

*Dehydration analysis*

Dehydration curves of the clay fractions are shown in Fig. 3. The curve of No. 7 looks very much like a dehydration curve of hydrated halloysite dried in air above 50 per cent $H_2SO_4$, but it shows slightly more adsorbed water than a typical hydrated

halloysite. It may be attributed to contamination by a small amount of allophane.

The sample No. 1 loses water approximately by 10 per cent below 110°C. and about 6 per cent between 420 and 490°C.. Assuming the latter water is due to hydrated halloysite, it may be estimated that there is about 50 per cent of hydrated halloysite in the No. 1 clay fraction, although it is not clear that the water is of hydrated halloysite alone or otherwise. Indeed, since hydrated halloysite and halloysite do not seem to be present so much in that fraction according to the results of X-ray diffraction analysis, a large part of the water must be attributed to other clay minerals. The curve, moreover, shows an appreciable amount of water volatilized at temperature between 110 and 400°C., agreeing with the results of the differential thermal analysis. It may be partly due to allophane, $R_2O_3$ hydrates, or others.

The curve of No. 6 differs in shape from other curves. It represents hygroscopic water amounting to over 14 per cent, a remarkable loss of water between 110 and 400°C., and a relatively small loss between 400 and 500°C., which does not happen so sharply as in the other samples.

### *Chemical analysis*

Chemical anlysis of clay fractions and bulk materials of weathered rocks were carried out after regulation of hygroscopic water as in previous experiments. Results obtained are given in Table 2.

The bulk chemical composition of No. 7 largely consists of silica, alumina, and water, the sum of them amounting to about 98 per cent. Neglecting other minor constituents, chemical formula is given as $2.00\ SiO_2 \cdot 1.05\ Al_2O_3 \cdot 3.30\ H_2O$. Since pure hydrated halloysite of Isshochi, Kumamoto Prefecture, has a formula $2\ SiO_2 \cdot Al_2O_3 \cdot 3.10\ H_2O$ under the same condition as above, the sample No. 7 seems to be mostly composed of hydrated halloysite.

The clay fraction of No. 2 is mainly composed of the three prominent constituents as No. 7 with a considerable quantity of iron, and

Table 2. Chemical composition of weathered rocks and their clay fractions (<2μ).

| | No. 1 | | No. 2 | | No. 6 | | No. 7 |
|---|---|---|---|---|---|---|---|
| | bulk | clay fr | bulk | clay fr. | bulk | clay fr. | bulk |
| $SiO_2$ | 46.82% | 43.59% | 48.48% | 41.44% | 39.28% | 38.64% | 41.02% |
| $Al_2O_3$ | 22.46 | 27.56 | 22.10 | 30.73 | 23.31 | 25.36 | 36.55 |
| $Fe_2O_3$ | 3.14 | 4.93 | 8.31 | 4.26 | 4.56 | 4.35 | 0.49 |
| MnO | 0.04 | 0.01 | 0.20 | 0.07 | 0.04 | 0.02 | tr. |
| MgO | 2.85 | 0.74 | 3.31 | 0.07 | 0.24 | 0.30 | tr. |
| CaO | 1.18 | 1.02 | 2.58 | 0.81 | 1.58 | 1.57 | 0.11 |
| $Na_2O$ | 0.47 | 0.72 | 0.32 | 0.15 | 0.26 | 0.10 | 0.04 |
| $K_2O$ | 0.25 | 0.37 | 0.17 | 0.19 | 0.19 | 0.10 | 0.11 |
| $TiO_2$ | 0.11 | 0.15 | 0.28 | 0.19 | 0.13 | 0.11 | tr. |
| $P_2O_5$ | 0.23 | 0.20 | 0.45 | 0.30 | 0.50 | 0.50 | tr. |
| $H_2O(+)$ | 10.16 | 11.40 | 4.84 | 12.34 | 12.40 | 13.28 | 13.66 |
| $H_2O(-)$ | 11.62 | 8.21 | 2.62 | 8.24 | 14.16 | 14.38 | 6.64 |
| Total | 98.61% | 97.81% | 93.17% | 98.45% | 96.20% | 98.51% | 98.47% |
| Free $Fe_2O_3$ | | 1.80% | | | | 3.73% | |
| Molecular ratio $SiO_2/Al_2O_3$ | 3.54 | 2.68 | 3.70 | 2.29 | 2.86 | 2.59 | 1.91 |
| $SiO_2/R_2O_3$ | 3.25 | 2.41 | 3.00 | 2.10 | 2.54 | 2.33 | 1.89 |

its molecular ratios $SiO_2/Al_2O_3$ and $SiO_2/R_2O_3$ are a little larger than 2, whereas the bulk composition contains more iron and alkali earths with higher ratios $SiO_2/Al_2O_3$ and $SiO_2/R_2O_3$ than the clay fraction. It seems that the clay fraction consists largely of hydrated halloysite with some iron hydrate, and the bulk contains some undecomposed fragments containing much iron, silica, magnesia, and lime.

Chemical composition of the clay fraction of No. 6 resembles very much the bulk of No. 6, and it is more or less true with No. 1. Molecular ratios $SiO_2/Al_2O_3$ in those clay fractions are 2.59 and 2.68, which may become higher to some extent than those figures, if allophane is excluded from the fractions. These clay fractions

contain considerable amount of combined iron and appreciable magnesia, which are sufficient to constitute octahedral layers of 2 : 1 type minerals. It would mean that No. 1 and No. 6 contain some montmorin presumably as rich in aluminum as beidellite in their clay fractions.

*Cation exchange, ethylene glycol retention and ammonium fixation*

Cation-exchange capacity, ethylene glycol retention, and ammonium fixation capacity were determined on the clay fractions as well as on the bulk materials of each sample (Table 3).

Table 3. Cation exchange, ethylene glycol retention and ammonium fixation by weathered rocks and their clay fractions.

| | No. 1 | | No. 2 | | No. 6 | | No. 7 |
|---|---|---|---|---|---|---|---|
| | bulk | clay fr. | bulk | clay fr. | bulk | clay fr. | bulk |
| Cation-exchange capacity (m.e./100gr.) | 51.4 | 61.9 | 20.3 | 45.6 | 66.6 | 88.4 | 20.9 |
| Ethylene glycol retention (mgr./gr.) | | | | | | | |
| Untreated | 105.8 | 124.3 | 91.0 | 106.0 | 127.2 | 186.4 | 73.2 |
| Heated at 600°C. | 32.3 | 30.8 | 9.8 | 39.3 | 58.7 | 88.9 | 18.7 |
| Difference | 73.5 | 93.5 | 81.2 | 66.7 | 68.5 | 97.4 | 54.5 |
| Ammonium fixation capacity (m.e./100gr) | | | | | | | |
| in wet state | 0.22 | | | | 0.48 | | 0.11 |
| in dried state | 5.35 | | | | 3.21 | | 1.61 |

The cation-exchange capacity of the clay fraction of No. 6 is so high that it is a match for that of montmorillonite or vermiculite. The capacity of No. 1 clay fraction is also too high for clay minerals other than montmorin and vermiculite, while the samples of the second group show a moderate capacity.

Amount of ethylene glycol retained by the clay fractions ranges from about 106 to 186 mgr. per one gram of dry matter for the untreated samples, and about 31 to 89 mgr. per one gram of dry matter for the heat-treated samples, and the difference between them

amounts to about 67 to 97 mgr./gr. which suggests the presence of some clay minerals retaining much ethylene glycol such as montmorillonite, allophane, or hydrated halloysite.

Ammonium fixation capacity was determined only for the bulk materials of the weathered rocks. As obvious in the Table 3, fixation of ammonium ions was recognized not only in the dry condition but also in the wet condition in all samples examined. The fixation in No. 1 and No. 6 may be explained as caused by some montmorin minerals in their clay fractions, because X-ray analyses indicate the presence of montmorin and other experiments substantiate this result.

No. 7, nearly pure hydrated halloysite, also showed appreciable fixation in the dry condition. The fixation of ammonium ions generally has been recognized to occur interlamellar in 2 : 1 type clay minerals[8)11)14)] although there are some observations against this explanation.[2)13)] It appears that some colloids other than 2 : 1 type minerals may fix ammonium ions in some conditions.

### *Electron microscopy*

Electron microscopic photographs of the clay fractions ($<2\,\mu$) are shown in Plates I and II. No. 1 contains irregular nebulous masses of various sizes with some tubular particles. No. 2 contains tabular particles, somewhat rounded but in general irregular shaped ones, and very small rounded ones about one fortieth of micron in diameter, which may be of allophane.

The clay fraction of No. 6 consists of particles of various shapes; tubular, nebulous, hair-like, very small rounded particles, and aggregates. The micrograph of No. 7 shows large tubular particles in majority with some small angular ones which probably are the fragments of the former.

The tubular particles found more or less in all samples may be safely said to belong halloysite or hydrated halloysite, but the species of other particles can not be determined solely through the observation of the microphotographs.

## *Summary and Conclusions*

It was suggested in a previous communication[3] by the present authors that montmorin in the clay fractions of the alluvial soils of the Chikugo River was derived from the upper stream due to flood water. Since the basin of the River is mainly composed of several lavas, the montmorin is supposed to be the weathering products of some volcanic rocks.

Weathered samples of an andesite and two agglomerates at Yoake, the oldest lavas in the basin, were examined for clay minerals by means of X-ray, thermal, chemical, and electron microscopic methods. Those agglomerates consist of fragments of two pyroxene andesite and thoroughly weathered white material, and fine-grained cementing matter. Those cementing matter as well as fragments of two pyroxene andesite contain predominant montmorin with hydrated halloysite and allophane, but white fragments are almost exclusively composed of hydrated halloysite. The decomposed andesite contains much hydrated halloysite and appreciable allophane in its clay fraction.

Montmorin found in the weathered agglomerates at Yoake seems to belong to an aluminian montmorillonite containing a little iron, magnesia, and potash. It loses lattice water below 500°C..

At least some parts of montmorin in the alluvial soils of the Chikugo River are hereby concluded to originate from decomposed agglomerates of the Tsukushi lava in the upper stream.

## *Acknowledgement*

The authors wish to express their hearty thanks for a grant from the Science Research Fund of the Japanese Ministry of Education for this work.

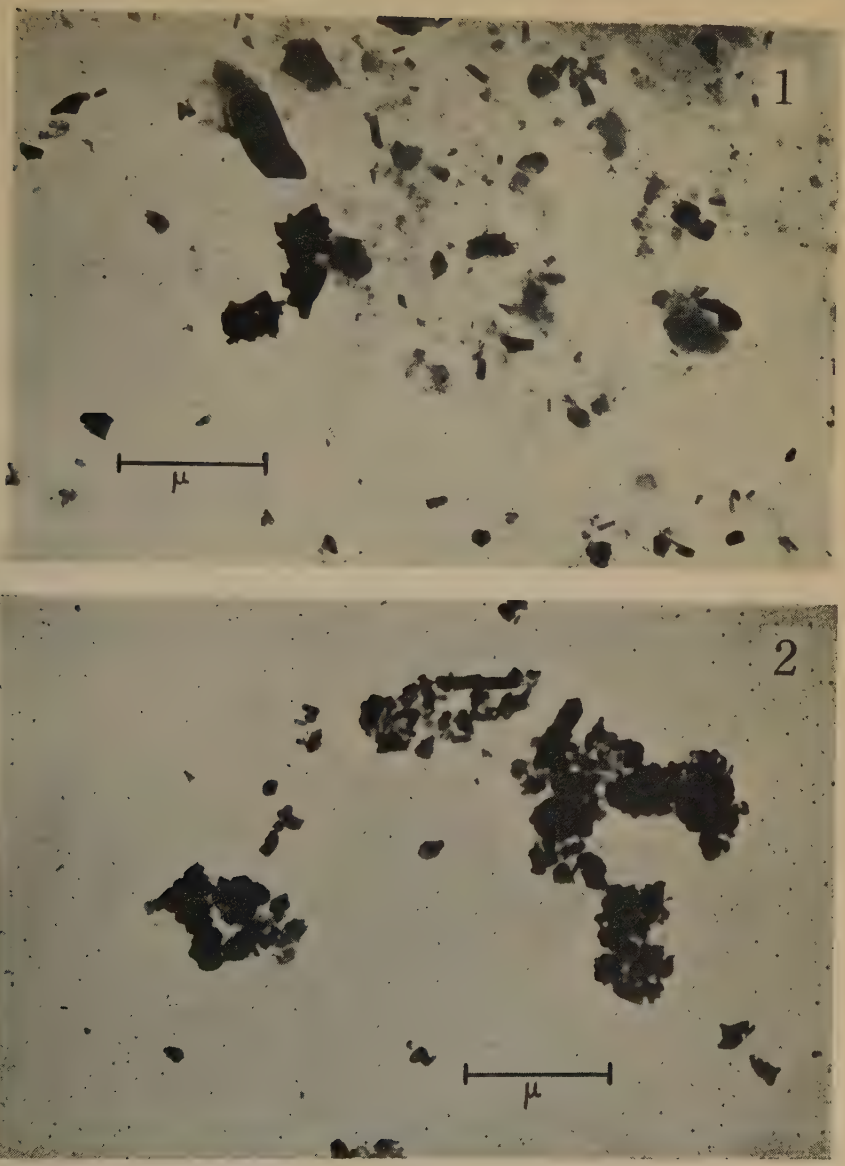


Electron micrographs of clay fractions (<2 μ)
1: clay fraction of the sample No. 1.
2: ditto, No. 2.

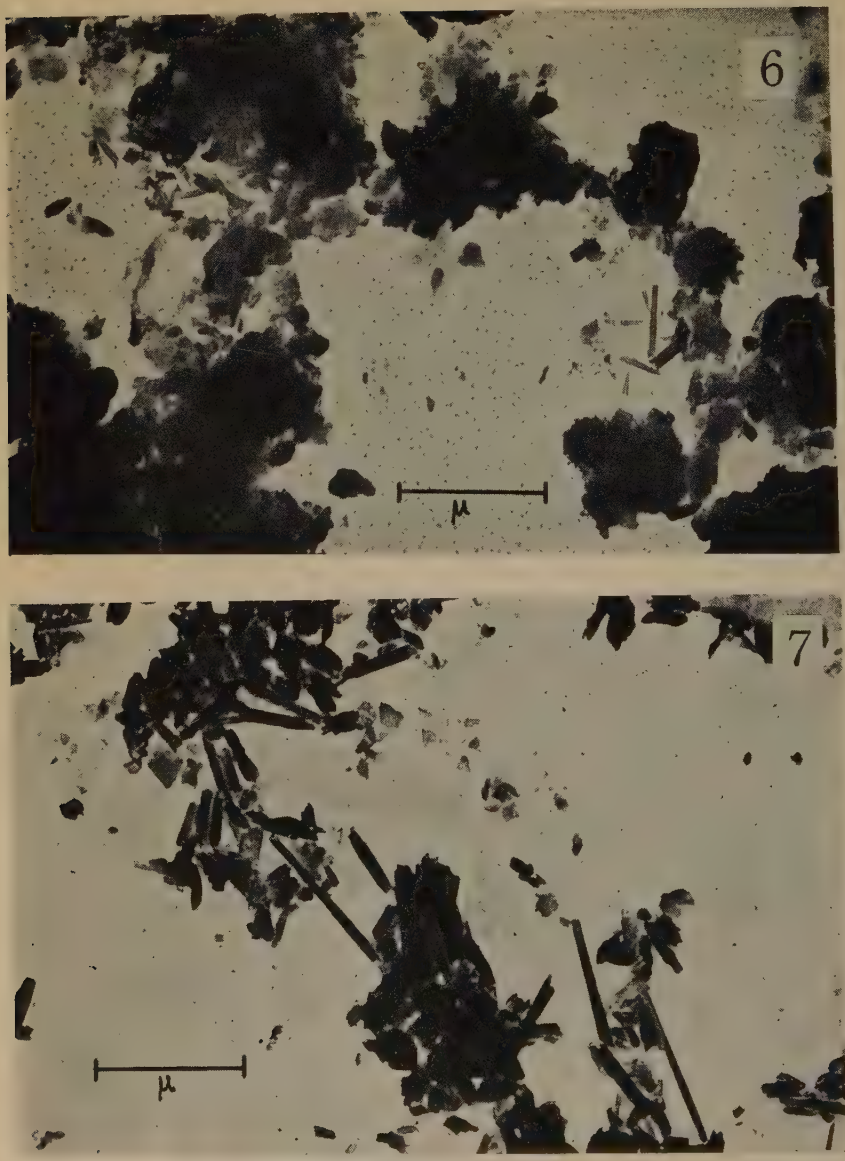


Electron micrographs of clay fractions (<2 μ)
6: clay fraction of the sample No. 6.
7: ditto, No. 7.

## REFERENCES

1) Akagi, T.: Geological Map of Mameda, 1: 75,000, and its Explanatory Text, Imp. Geol. Surv. Japan (1934).
2) Allison, F. E., M. Kefauver, and E. M. Roller: Soil Sci. Soc. Amer., Proc., **17**, 107 (1953).
3) Aomine, S. and T. Higashi: Jour. Fac. Agr. Kyushu Uuiv., **10**, 355 (1956).
4) Aomine, S. and K. Wada: Clay minerals derived from weathering of pumice in Aso district (unpublished).
5) Aomine, S. and N, Yoshinaga: Soil Sci., **79**, 349 (1955).
6) Dyal, R. S. and S. B. Hendricks: Soil Sci., **69**, 421 (1950).
7) Egawa, T., Y. Watanabe, and A. Sato: Bull. Nat. Inst. Agric. Sci., B. **5**, 39 (1955).
8) Joffe, J. S. and A. K. Levine: Soil Sci., **63**, 151 (1947).
9) Martin, R. T.: Soil Sci. Soc. Amer., Proc., **19**, 160 (1955).
10) Martin, R. T. and M. B. Russell: Soil Sci., **74**, 264 (1953).
11) Page, J. B. and L. D. Baver: Soil Sci. Soc. Amer., Proc., **4**, 150 (1939).
12) Sudo, T. and J. Ossaka: Jap. Jour. Geol. Geogr., **22**, 215 (1952).
13) Volk, G. W.: Soil Sci., **45**, 263 (1938).
14) Wear, I. and J. L. White: Soil Sci., **71**, 1 (1951).

*Manuscript received June 22, 1955.*

MINERALOGICAL JOURNAL, VOL. 1, NO. 5, PP. 290-302, DEC., 1955

# ON THE ELECTRICAL CONDUCTION OF PYRITE*

AKIRA SASAKI

*Geological Institute, Faculty of Science, University of Tokyo.*

ABSTRACT

Electrical resistivity of pyrite has been measured over the wide temperature range from about −180°C to +400°C on some specimens from Japan. The data obtained show that the electrical conduction of natural pyrite possesses the properties of typical extrinsic semiconductor. The presence of some impurity energy levels causes rather low and various resistivities at room temperature, while the perfect crystal without such impurity energy levels should have the higher specific resistivity, about $10^4$ Ωcm.. Some features of the impurity energy levels which are responsible for the extrinsic semiconduction are also discussed, but the origin of such levels is still unknown.

## *Introduction*

Electrical properties of pyrite as well as the other electrical conducting minerals have been studied from the beginning of the 19th century[6),7)]. Through these early investigations the dispersive character of electrical properties was mostly interested. Towards 1940, F.G. Smith[14)] investigated comprehensively the variation of electrical resistivity and thermal electromotive force of pyrite, and postulated the idea of "pyrite geo-thermometer" in 1947.[15)] Although similar works have been carried out by some investigators[3),18),4),9),2)] since then, lack of basic knowledge of electrical behaviour of the mineral has prevented the proper interpretation or discussion of data.

The present work was undertaken to reveal the characters of the electrical conduction of pyrite, which are indispensable to the

* Read at the meetings of the Geological Society of Japan on April 30, 1954 and April 6, 1955.[11)]

further mineralogical or geological interpretations of this property. For this purpose the author carried out measurements of the electrical resistivity and the sign of thermal electromotive force over the temperature range from about −180°C to +400°C on specimens whose homogeneity had been examined carefully.

Recently, after our experimental works had been finished, J.C. Marinace[5] reported the electrical resistivity and Hall efect of pyrite. The results obtained by the author agree qualitatively with those by Marinace.

## *Experimental Procedure*

Specimens were sawed from well-formed single crystals, which were ascertained previously to be free from inclusions by X-ray powder method, into small prisms approximately $0.1 \times 0.2 \times 0.5$ cm. in dimensions. Their surfaces were smoothed by lapping with 600 mesh carborundum and water.

The measuring circuit and the details of some equipments are illustrated in Fig. 1. The resistivity was measured by the potential probe method, and the temperature by the thermoelectric voltage of a copper-constantan thermocouple. A potentiometer in conjunction with a selector switch was used to measure both of these direct current voltages (Fig. 1 A).

In order to cover the temperature range from about −180°C to +400°C two different temperature controlling units were employed. The apparatus shown in Fig. 1 B was used below room temperature, while that in Fig. 1 C above room temperature. On both cases desired temperatures were obtained by heating coils operated manually with variac, and measurements were carried out in an atmosphere of air. The upper limit of temperature, about +400°C, was chosen to avoid the marked oxidation of this mineral.

A sample holder shown in Fig. 1 D was used over the entire temperature range. Copper plate was used as the current electrodes on

which the specimen was spanned and pressed with the spring action of tungsten or phosphor bronze wire. The potential probe was also prepared by the same materials. The current through the specimen, usually between 2 and 4 mA., was supplied from a simple constant current source illustrated in Fig. 1 A. To eliminate spurious effect originating from thermal electromotive force two potential difference

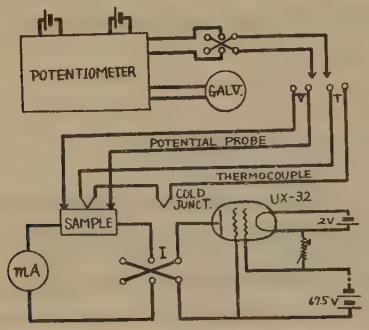


(A)

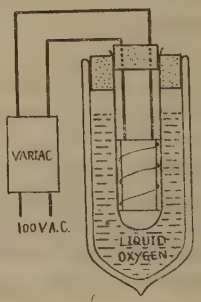


(B)

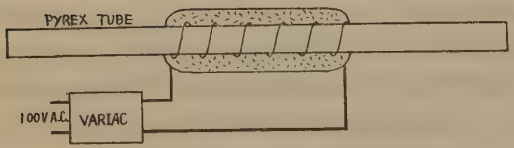


(C)

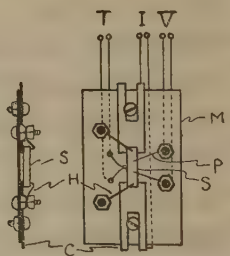


(D)

Fig. 1. Circuit and apparatus for measuring resistivity.
(A) : Circuit diagram.
(B) : Apparatus for low temperature control.
(C) : Apparatus for high temperature control.
(D) : Sample holder.

data $\varphi$ and $\varphi'$ were obtained for each specimen with mutually opposite directions of the same current $i$, and the specific resistivity $\rho$ is calculated from the following equation,

$$\rho=\frac{s}{l}\times\frac{\varphi-\varphi'}{2i}, \qquad (1)$$

where $s$ is the cross section of prism and $l$ is the distance between two potential probes, $\varphi$ and $\varphi'$ are potentials of one potential probe relative to the other.

The sign of thermal electromotive force of the specimen was determined prior to the resistivity measurement. When a specimen had been settled on the holder, galvanometer was connected to the terminal V in Fig. 1 A, and thermal gradient was produced by bringing a small heated metal rod close to one end of the specimen. The direction of thermal electric current was determined from deflection of galvanometer. The sign of thermal electromotive force is taken as positive when the thermal electric current flows in the same direction as the thermal current in the specimen.

Electrical homogeneity of each specimen was also carefully examined to avoid false result due to mechanical cracks or impure phases etc., by surveying the potential distribution produced in a specimen when stational current was supplied at any definite temperature. A convenient arrangement, mainly composed of the microscope with mechanical stage and the similar sample holder as described above, was devised for this object. Fig. 2 provides some examples of the results of homogeneity examination. The potential difference, which was read at every 0.05 mm. along the lines indicated in Fig. 2, is plotted against the distance from a standard point. If the specimen is highly homogeneous the potential versus distance plot should give a straight line with a slope proportional to its resistivity with some exclusive disarrangements near the current electrodes. Obtained results, however, show the more or less complicated curves. Figs. 2A, 2B, and 2C exemplify respectively the specimens fit, just fit, and unfit for resistivity measurement.

The resistivity measurement was performed on the homogeneous part of the specimen, as indicated in Fig. 2A or Fig. 2B. Usually,

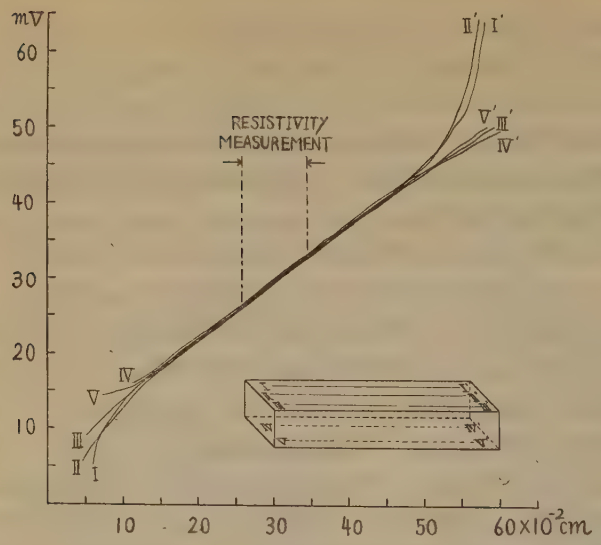


Fig. 2A. Electrical homogeneity of a specimen fit for resistivity measurement.

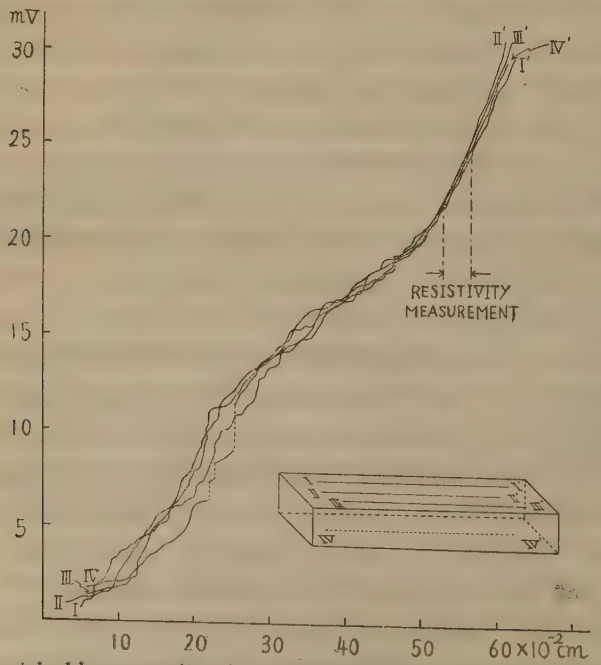


Fig. 2B. Electrical homogeneity of a specimen just fit for resistivity measurement.

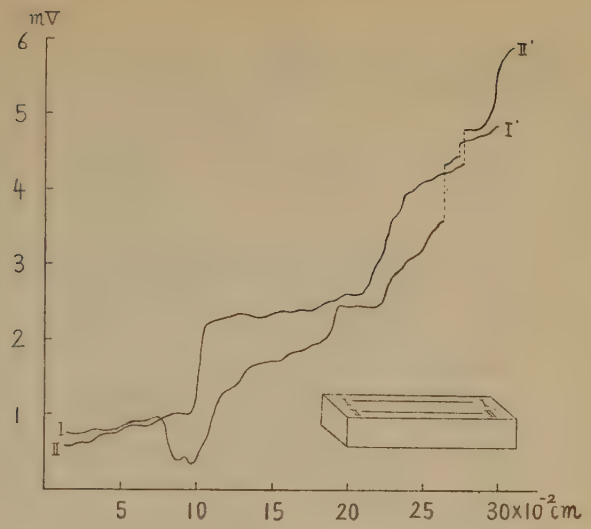


Fig. 2C. Electrical homogeneity of a specimen unfit for resistivity measurement.

the distance between potential probes could not exceed 1 mm., because of poor homogeneity of specimen. So far as the homogeneity of specimen has been strictly examined, the results of resistivity measurement are highly reproducible.

It must be noticed, however, that the homogeneity examination above described can not reveal such inhomogeneity as due to layers with different resistivity, parallel to the current.

### *Experimental results*

The experimental results are summarized in Table 1 and Fig. 3. In Table 1 the specific resistivities at 20°C of twenty one specimens are shown together with the sign of temperature coefficient of resistivity and the sign of thermal electromotive force, determined at room temperature. Some descriptions on locality of specimen, crystallographic direction of measurement, and crystal habit are tabulated as well. The meaning of p or n will become clear in the

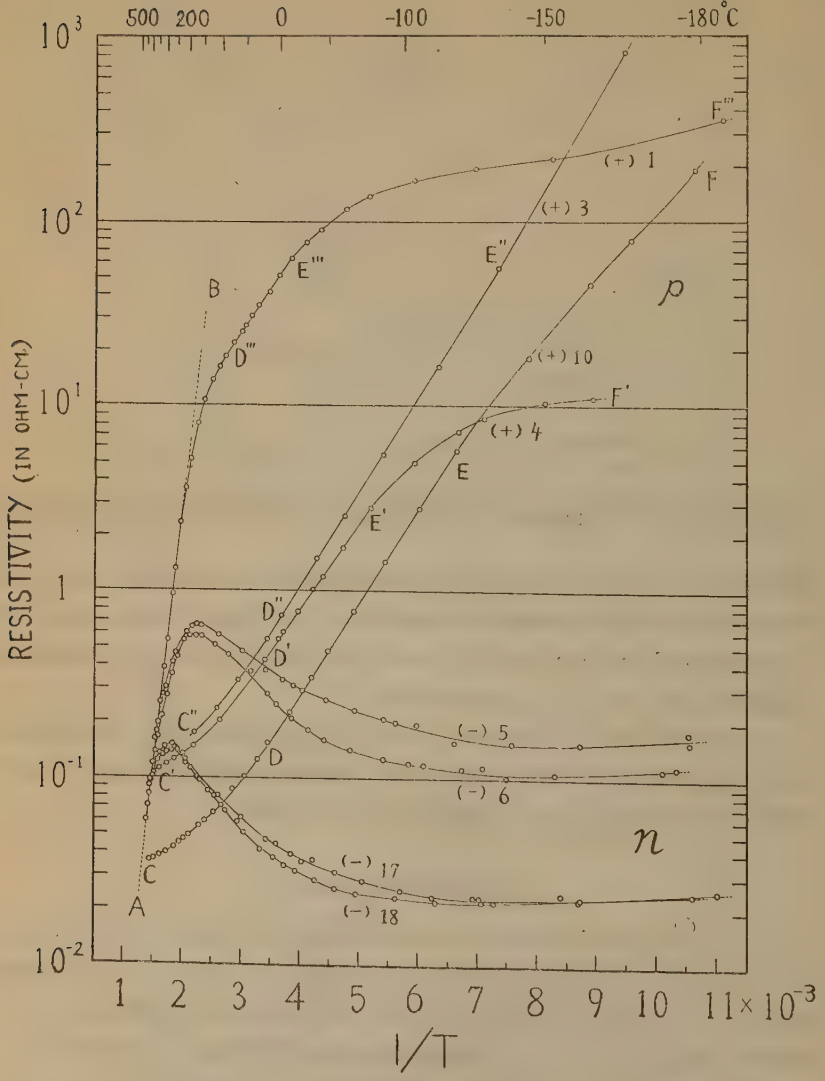


Fig. 3. Resistivity of pyrites as a function of the inverse absolute temperature.

Table 1. Specific resistivity of pyrites at 20°C. (in

| No. of Specimen | Crystallographic direction of measurement | Specific resistivity $\rho$ ($\Omega$cm) at 20°C | Sign of temperature coefficient of resistivity at room temperature | Sign of thermal e.m.f. at room temperature | Type of Conducti |
|---|---|---|---|---|---|
| 1 | [100] | $(3.8\pm0.2)\times10^{1}$ | − | + | p |
| 2 | [100] | $(9.3\pm1.8)\times10^{-1}$ | − | + | p |
| 3 | [100] | $(5.1\pm0.2)\times10^{-1}$ | − | + | p |
| 4 | [100] | $(4.3\pm0.2)\times10^{-1}$ | − | + | p |
| 5 | [100] | $(3.9\pm0.2)\times10^{-1}$ | + | − | n |
| 6 | — | $(2.9\pm0.2)\times10^{-1}$ | + | − | n |
| 7 | [110] | $(2.7\pm0.2)\times10^{-1}$ | − | + | p |
| 8 | — | $(2.4\pm0.4)\times10^{-1}$ | + | − | n |
| 9 | — | $(1.6\pm0.5)\times10^{-1}$ | + | − | n |
| 10 | [111] | $(1.4\pm0.3)\times10^{-1}$ | − | + | p |
| 11 | [110] | $(1.4\pm0.2)\times10^{-1}$ | − | + | p |
| 12 | — | $(1.3\pm0.3)\times10^{-1}$ | + | − | n |
| 13 | [100] | $(1.1\pm0.3)\times10^{-1}$ | + | − | n |
| 14 | [100] | $(7.4\pm0.6)\times10^{-2}$ | + | − | n |
| 15 | — | $(6.4\pm0.4)\times10^{-2}$ | + | − | n |
| 16 | [100] | $(5.6\pm0.9)\times10^{-2}$ | + | − | n |
| 17 | [111] | $(4.9\pm0.3)\times10^{-2}$ | + | − | n |
| 18 | — | $(4.0\pm0.3)\times10^{-2}$ | + | − | n |
| 19 | [100] | $(3.9\pm0.3)\times10^{-2}$ | + | − | n |
| 20 | — | $(2.2\pm0.4)\times10^{-2}$ | + | − | n |
| 21 | [100] | $(2.9\pm0.6)\times10^{-3}$ | + | − | n |

* Copper-quartz vein, shallow type.
** Massive ore body of hematite, pyrite, and sphalerite, associating with
*** Stibnite-sericite-quartz vein, shallow type.
**** Gypsum ore body near the margin of "Kuroko" deposit.
***** Tin-tungsten-quartz vein, deep type.
****** "Yellow ore" body in "Kuroko" deposit.
******* Pyrite-barite vein near the margin of "Kuroko" deposit.

next section.

The full features of the temperature dependence of resistivity are provided in Fig. 3, in which the resistivities are plotted logarithmically against the inverse absolute temperature. Celsius scale is added on the top end of the Figure. The number accompanied to each curve corresponds to the specimen number in Table 1. The sign + or − indicates the sign of thermal electromotive force at room temperature.

Among the experimental results following features may be noticeable.

As shown in Table 1 or Fig. 3, the dispersive character of data in lower temperature range is remarkable. The specific resistivity at 20°C is distributed between the order of $10^{-3}\Omega$cm. and $10^{1}\ \Omega$cm.. Both positive and negative sign of thermal electromotive force are observable. Generally speaking, the higher resistivity is accompanied with the positive sign of thermal electromotive force, and the lower resistivity with the negative sign.

The temperature dependence of resistivity in Fig. 3 has two quite different tendencies and has an apparent correlation to the sign of thermal electromotive force. The resistivity of the specimen with positive thermal electromotive force always decreases with the increase of temperature over the entire temperature range. The resistivity of the specimen with negative thermal electromotive force shows, however, slowly decreasing, increasing, and rapidly decreasing tendencies in the lower, medium, and higher temperature ranges respectively, with the increase of temperature. Therefore, at room temperature, the former has usually negative and the latter has usually positive coefficient of the temperature dependence of resistivity, as shown in Table 1.

In Fig. 3 the lineality of the resistivity variance is observable in the portions denoted by A-B, D-E, D′-E′, D″-E″, and D‴-E‴.

At high temperatures the temperature dependence of resistivity

of all specimens appears to follow the same variation curve along the line A-B, in spite of the dispersive character at lower temperatures. Moreover, in this temperature range all specimens show negative sign of thermal electromotive force.

These are typical features for semiconductors.[8),12),16),19)]

### *Analysis of data*

As noticed above, at high temperatures the resistivity of all specimens tends to follow the same variation diagram, A-B in Fig. 3, independent of their dispersive character over the lower temperature range. The conduction in the temperature range A-B is certainly so-called intrinsic, and the rapid decrease of resistivity with increasing temperature results from the increase in concentration of electrons and holes which arise due to thermal excitation of electrons from the filled to the conduction band.

Electrical resistivity $\rho$ of semiconductors is expressed by

$$\rho=\frac{1}{e(n_1b_1+n_2b_2)}, \qquad (2)$$

where $e$ is the magnitude of electronic charge, $n_1$ or $n_2$ the concentration of current carriers, and $b_1$ or $b_2$ the mobility of current carriers. The subscripts 1 and 2 denote conduction electrons and holes respectively. In equation (2), both concentrations and mobilities vary with temperature. Theory indicates that the following approximation is generally allowable in intrinsic region[1)],

$$n_1=n_2=n=N_0 \exp(-E_g/2kT), \qquad (3)$$

where $N_0$ is a factor scarcely dependent on temperature, $E_g$ the width of the forbidden band, or the gap in energy between the highest filled band and the lowest empty band, $k$ Boltzmann's constant, and $T$ the absolute temperature. Usually the mobilities depend far less on temperature than the carrier concentrations in intrinsic region, so the temperature dependence of resistivity is almost

entirely due to the variation of $n$ with temperature. Hence, the temperature dependence of resistivity is approximated by

$$\rho = A \exp(E_g/2kT), \qquad (4)$$

where $A$ is a material constant independent on temperature. Equation (4) gives a straight line in log $\rho$ versus $1/T$ plot. The line A-B in Fig. 3 conforms to equation (4) with $E_g$=1.12 eV. and $A \approx 5 \times 10^{-6}\Omega$ cm.. The values of $A$ and $E_g$ should be the constants for a definite mineral species, and are independent on impurities responsible to low temperature conduction.

If the crystal were perfect structurally as well as chemically, the resistivity at lower temperatures would be expressed by the extrapolation of the line A-B. It indicates the value of about $2.5 \times 10^4\,\Omega$ cm. at 20°C.. All of the specimens examined here, however, do not follow the line A-B at lower teperatures and show the exceedingly lower resistivities (Table 1). The electrical conduction at those lower temperatures is regarded as due to excited carriers from impurities and is generally called extrinsic. There are two types of extrinsic conduction, p type and n-type. In p-type the current is carried mainly by holes excited from acceptors into the filled band, and in n-type by electrons excited from donators into empty band. The symbols p and n in Table 1 and Fig. 3 indicate the type of conduction determined from the sign of thermal electromotive force.

In an extrinsic semiconductor carriers of one type predominate and equation (2) becomes,

$$\rho = \frac{1}{enb} = \frac{1}{ebn_0 \exp(-\Delta E/2kT)}, \qquad (5)$$

where $n$ is the concentration of the predominant carriers, $b$ their mobility, $n_0$ a factor related with the concentration of impurities but scarcely dependent on temperature, and $\Delta E$ the energy difference of the impurity level and the band edge.

If the temperature dependence of $b$ is small compared to that of $n$,

or exp $(-\Delta E/2kT)$, the log $\rho$ versus $1/T$ plot should give a straight line. This is the case of p-type specimens in Fig. 3, denoted by D–E, D′–E′, D″–E″, and D‴–E‴, with $\Delta E$ of acceptors, $\Delta E_p = 0.20 \pm 0.01$ eV..

If the temperature dependence of $n$ is very small, the temperature dependence of resistivity is determined by that of $b$. This is the case of n-type specimens in Fig. 3. In this case $\Delta E$ of donators, $\Delta E_n$, is small compared to $kT$, and can not be estimated from the gradient of log $\rho$ versus $1/T$ plots.

The curves of p-type specimens deviate from straight lines (E′–F′, E‴–F‴) and cross mutually (E–F and E′–F′, E″–F″ and E‴–F‴) in lower temperature range of extrinsic conduction. It seems that there are two possible factors in these features. One is the existence of two kinds of acceptors with different $\Delta E$ in the specimens 1 and 4. The other is the existence of thin n-type layer, which is indetectable by the homogeneity examination as has been noticed in the experimental procedure section, in mostly p-type specimens 1 and 4.

From the analysis stated above, the energy level diagram which is responsible to the electrical conduction of natural pyrite is schematically constructed in Fig. 4. It has to be mentioned here that the energy constants shown in Fig. 4 were calculated from the resistivity data. To provide the more accurate energy relations measurement of the temperature dependece of Hall effect are desirable.

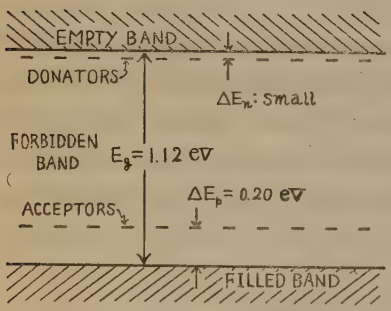


Fig. 4. Schematic energy level diagram for pyrite.

The fact that all specimens have negative thermal electromotive force in intrinsic region shows that the mobility of electron is higher than that of hole.[10]

*Discussions*

The prevailing electrical inhomogeneities revealed by the author's strict examination may be partly due to the presence of mechanical cracks or impure phases, and partly due to the variation of the concentration of impurities in a specimen. The variation of electrical properties in a single crystal or among many crystals of pyrite calls our attention to its genetical meaning. In order to clarify it, however, we must carry out much basic investigations further on.

Except some early investigations almost all the specific resistivity data reported in literatures[6),7),13),14),11),4)] give the more or less lower resistivity values at room temperature compared with $10^4\ \Omega$ cm., the room temperature intrinsic resistivity of pyrite. Therefore, it seems that most of natural pyrites show extrinsic conduction at room temperature.

As mentioned already and also pointed out by some investigators[14),4)] there is a tendency that the resistivities of n-type specimens are lower than that of p-type specimens. This is partly due to the higher mobility of electrons in extrinsic region[5)] and smaller $\Delta E$ of donators.

The room temperature mobility of electron in pyrite was estimated by Marinace[5)] to be about $1\times10^2$ cm$^2$/volt. sec.. Then, for example, the carrier concentration of the most impure n-type specimen (No. 21) is roughly estimated as $10^{19}$/cc. by equation (5), equivalent to one conduction electron per $10^4$ atoms. This figure applies to donator concentration, since $\Delta E_n$ is very small and the donators are mostly ionized at room temperature. This diluteness of impurity concentration must be noted in the speculation of the origin of impurities.

It is an essential problem to reveal the origin of impurities. Since the direct detection of impurities by usual chemical method may be very difficult owing to their diluteness, artificial preparation of intrinsic single crystals of pyrite is hoped to be doped with known quantities of various impurities.

*Acknowledgements*

The author wishes to express his sincere thanks to Prof. T. Watanabe and Prof. T. Sudo for their kind interest and stimulating advices. He owes to Mrs. T. Aoki, M. Kimura, T. Miyake, H. Mukaiyama, T. Nitta, Y. Okubo, K. Sakura, M. Sato, S. Tono and Dr. T. Tatsumi for offering specimens. He also wishes to express his thanks to Dr. K. Hayase, Mr. R. Otsuka, Mr. T. Miyake, and Dr. T. Tatsumi for their interest in this work.

This work was financially supported by the Grant in Aid for Scientific Researches from the Ministry of Education, Japan.

## References

1) Fowler, R. H.: Statistical Mechanics, London (1936).
2) Harada, Z. & Y. Hariya: Mineral. Jour., 1, 97 (1954).
3) Hashimoto, S.: Misc. Rep. Res. Inst. Natur. Resourses, 24, 28 (1951).
4) Hayase, K. & R. Otsuka: Jour. Geol. Soc. Japan, 58, 133, 497 (1952); 59, 469 (1953).
5) Marinace, J. C.: Phys. Rev., 96, 593 (1954).
6) Mellor, J. W.: Comprehensive treatise of inorganic and theoretical chemistry, No. 14 (1935).
7) Meyer, R. J.: Gmellins Handbuch der Anorganishen Chemie, Nr. 59 (1930).
8) Mott, N. F. and R. W. Gurney: Electronic Processes in Ionic Crystals, London (1940).
9) Mutch, A. D.: Min. Eng., 4, 880 (1952).
10) Pearson, G. L. and J. Bardeen: Phys. Rev., 75, 865 (1949).
11) Sasaki, A,: Jour. Geol. Soc. Japan, 60, 293 (1954); 61, 316 (1955).
12) Seitz, F.: Modern Theory of Solids, New York (1940).
13) Slichter, L. B. and M. Telkes: Handb. Phys. Constants, Geol. Soc. Amer., Spec. Papers, 36, 229 (1942).
14) Smith, F. G.: Univ. Tronto Studies, Geol. Ser., 44, 83 (1940); Amer. Mineral., 27, 1 (1942); Econ. Geol., 37, 519 (1942).
15) ——: Econ. Geol., 42, 515 (1947).
16) Stöckmann, F.: Forts. d. Mineral., 33, 1 (1954).
17) Telkes, M.: Amer. Mineral., 35, 536 (1950).
18) Watanabe, Y., Nishizawa, J. and I. Sunagawa: Kagaku, 21, 140 (1951).
19) Wilson, A. H.: Semiconductors and Metals, London (1939).

*Manuscript received July 29, 1955.*

MINERALOGICAL JOURNAL, VOL. 1, NO. 5, pp. 303-312, DEC., 1955

# THE NUMBER OF COUNTS OF BETA-RAYS DETECTED BY AN END WINDOW GEIGER-MUELLER COUNTER (PART II)*

NOBUO KATAYAMA

*Institute of Earth Science, College of General Education, University of Tokyo*

ABSTRACT

The formulae for the number of counts per minute of beta-rays ejected from homogeneous rocks or ores and detected by an end-window Geiger-Mueller counter at a distance more than four centimetres have been calculated with the results as follows:

$$T=\frac{60\pi pNW}{C^*}G,$$

where

$$G=e^{-\frac{\mu_A^* H}{[\cos\delta]}}g,$$

$$g=\left(\tan^{-1}\frac{H^2+x_1^2}{XH}-\tan^{-1}\frac{H}{X}\right)\frac{XH}{4},$$

or

$$g=\left(\frac{1}{H^2}-\frac{1}{H^2+X_1^2}\right)S_0H^4,$$

and $\mu_A^*$: the absorption coefficient for air regarding the number of beta-rays ($cm^{-1}$),

$[\cos\delta]$: the mean velue of $\cos\delta$,

$S_0$: the effective solid angle at the point in which the extension of the central line of Geiger-Mueller tube meets the surface of the object,

other notations being the same as in the previous report.

---

* Read at the Annual Meeting of the Mineralogical Society of Japan held in Tokyo on June 3, 1955.

## *Introduction*

In his previous report[1] the writer introduced a formula for calculating the number of counts per munite of beta-rays detected by an end-window Geiger-Mueller counter as follows:

$$T=\frac{60\pi pNW}{C^*}\sum_n G_{(n,n+1)}, \qquad (15)$$

where $p$: the content of a beta-radioactive isotope (in decimal),
$n$: the number of beta-rays emitted by the beta-radioactive isotope per gram per second,
$W$: a term representing the absorption effect due to the substaces between the sample and the sensitive volume of the counter,
$C^*$: the mass absorption coefficient for any substance regarding the number of the beta-rays ($cm^2\ gr^{-1}$),
and $\Sigma G_{(n,n+1)}$: calculated from the geometrical relation of apparatus and procedure as well as the absorption coefficient of the beta-ray for the sample.

The calculated values are in good agreement with the results of measurement when the distance between the counter and the sample is short.

As we have to measure in the field with a rather long distance between the counter and the object, and as the distance we prefer usually is about ten centimetres owing to the roughness of surface and the heterogeneity of the object, the writer has tried to extend calculation with the view that the results may adequately represent the actual counting.

## *Effective solid angle*

Denote by $S$ the effective solid angle, that is, the solid angle of the cone, the vertex of which is the point source of beta-ray and the base the basal section of the sensitive volume of the counter,

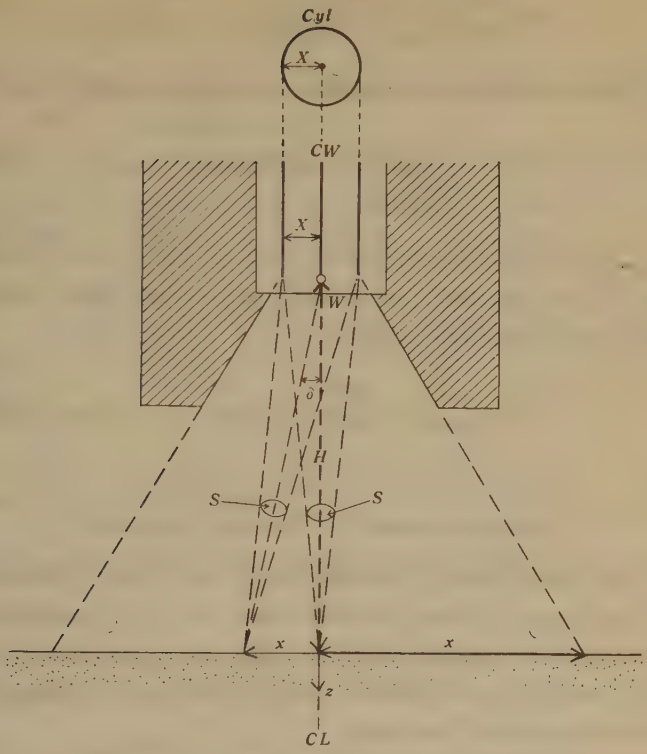


Fig. 5. Scheme of measurement of beta-rays in the field.
Cyl: cylinder cathode. CW: central wire.
W: window, CL: central line.

as designated in the previous paper[1] (Fig. 5). Since the value of $H$, the distance between the end point of central wire and the surface of the object exceeds by far the value of $X$, the radius of the basal section of the sensitive volume, in this case, the effective solid angle may be expressed approximately as follows:

$$S \fallingdotseq \frac{\pi X \cdot X \cos\delta}{4\pi (H^2 + x^2 + X^2 \cos^2\delta)} \qquad (20)$$

Substituting $\cos\delta$ by $\frac{H}{\sqrt{H^2+x^2}}$, we get

$$S \fallingdotseq \frac{X^2 H \sqrt{H^2+x^2}}{4\{(H^2+x^2)^2+X^2H^2\}} . \tag{21}$$

If the value of $H$ is large enough, $S$ may be expressed as follows:

$$S \fallingdotseq \frac{\pi X \cdot X \cos\delta}{4\pi \frac{H^2}{\cos^2\delta}} = S_0 \cos^3\delta, \tag{22}$$

where $S_0$ denotes the effective solid angle at the point in which the extension of the central line of Geiger-Mueller tube meets the surface of the object, and is given by

$$S_0 \fallingdotseq \frac{\pi X^2}{4\pi H^2} = \frac{X^2}{4H^2} . \tag{23}$$

*Number of counts of beta-rays detected*

Since the solid angle is rather small, the mean declination of tracks of beta-ray, $D$, may be substituted by $\delta$ for approximation. Then, assigning a suitable value to $z_1$ so that $S$ and $\cos\delta$ can be regarded practically as constant between $z=0$ and $z_1$, equality (9) in the previous paper[1] becomes,

$$dU_z = 2\pi x\, dx \cdot \frac{pN}{C^*} S \cos\delta \left(1-e^{-\frac{\mu^* z_1}{\cos\delta}}\right), \tag{24}$$

where $dU_z$ denotes the differential of the number of effective beta-rays per second ejected from the layer between $z=0$ and $z_1$, and $\mu^*$, the absorption coefficient for the substance to be measured regarding the number of the beta-rays.

In the previous calculation the absorption of beta-rays by the air between the counter and the sample was neglected, because we treated exclusively of the case with rather small values of $H$. But, in the field we cannot neglect the absorption by air. Hence, introducing the absorption term for air, and applying equalities (21) and (24), $G$ in equality (15) is given by

$$G=\frac{1}{2}\int_0^{x_1}\frac{X^2H^2}{(H^2+x^2)^2+X^2H^2}\left[1-e^{-\frac{\mu^* z_1}{\cos\delta}}\right]e^{-\frac{\mu_A^* H}{\cos\delta}}xdx, \qquad (25)$$

where $\mu_A^*$: absorption coefficient for air regarding the number of beta-rays ($cm^{-1}$).

Since the values of absorption terms do not vary so much within the limitting values of $x$, they may be regarded as a constant which is represented by the mean value of $\cos\delta$ given by

$$[\cos\delta]=\frac{\int_0^{x_1}\frac{H}{\sqrt{H^2+x^2}}\cdot 2\pi xdx}{\pi x_1^2}=\frac{2H(\sqrt{H^2+x_1^2}-H)}{x_1^2}. \qquad (26)$$

Hence, equality (25) becomes,

$$G=e^{-\frac{\mu_A^* H}{[\cos\delta]}}\left(1-e^{-\frac{\mu^* z_1}{[\cos\delta]}}\right)\left(\tan^{-1}\frac{H^2+x^2}{XH}-\tan^{-1}\frac{H}{X}\right)\frac{XH}{4}. \qquad (27)$$

If the value of $H$ is large enough, using equality (22) instead of (21) we get

$$G=2\int_0^{x_1}S_0\cos^4\delta\left(1-e^{-\frac{\mu^* z_1}{[\cos\delta]}}\right)e^{-\frac{\mu_A^* H}{[\cos\delta]}}xdx. \qquad (28)$$

Substituting $\cos\delta$ by $\frac{H}{\sqrt{H^2+x^2}}$, we get

$$G=e^{-\frac{\mu_A^* H}{[\cos\delta]}}\left(1-e^{-\frac{\mu^* z_1}{[\cos\delta]}}\right)\left(\frac{1}{H^2}-\frac{1}{H^2+x_1^2}\right)S_0H^4. \qquad (29)$$

*Numerical calculations for rocks and ores*

As evident from the Table 2 in the previous paper[1], the increase of $G$ with the thickness of rocks and substances with comparable density becomes stationary by the layer thinner than four millimetres. In the case the value of $H$ is larger than four centimetres, $S$ and $\cos\delta$ being regarded as constant between $z=0$ and four millimetres, $G$ is given by

$$G=e^{-\frac{\mu_A^* H}{[\cos\delta]}}g, \qquad (30)$$

where
$$g=\left(\tan^{-1}\frac{H^2+x_1^2}{XH}-\tan^{-1}\frac{H}{X}\right)\frac{XH}{4}, \qquad (31\text{-}1)$$

or
$$g=\left(\frac{1}{H^2}-\frac{1}{H^2+x_1^2}\right)S_0H^4. \qquad (31\text{-}2)$$

The numerical values of $g$ are calculated for the cases $H$=4.5 cm., 5.5 cm., 10 cm. and 100 cm.. $X$=1 cm., and $x_1$=1+0.6 $H$ cm. for every case. These values were assigned in accordance with the apparatus and procedure designed by the present author[3] (Fig. 5). The results are shown in Table 3.

Table 3. Calculated value of $g$.

| $H$ (cm.) | 4.5 | 5.5 | 10 | 100 |
|---|---|---|---|---|
| $g$ | 0.098 | 0.092 | 0.081 | 0.068 |

Regarding the beta-ray of $K^{40}$, the value of $C^*$ having been determined as 9.1[1], we may assume, for the time being, the value of $\mu_A^*$ to be 0.0109, assigning for $\rho^*$ the normal density of air. As for the beta-rays emitted from isotopes belonging to the uranium family or to the thorium family, the values of $\mu_A^*$ were estimated with reference to their usual absorption and the value of $\mu_A^*$ for $K^{40}$. Thus the numerical value of $G$ for each beta-radioactive isotope was calculated according to equality (30).

In the expression for $T$ in equality (15), $pN$i s a constant for each family, if its members are in radioactive equilibrium with each other. In such cases, the particular term for each isotope is $\frac{W}{C^*}G$, of which $C^*$ can be estimated in the same way as $\mu_A^*$, and $W$ can be calculated as $e^{-\frac{C^*\sigma}{[\cos\delta]}}$ which expresses the absorption effect of the mica window[1].

The numerical value of $\frac{W}{C^*}G$ for each beta-radioactive isotope is tabulated in Table 4. UZ, RaC″ anb AcC are omitted because their beta-radioactivity is small among the uranium family. RaD and $MsTh_1$ too, are omitted because the energy of their beta-rays is too weak to be detected at such a distance as indicated in Table 4.

Table 4. The numerical value of $\frac{W}{C^*}G$ for beta-rays emitted from natural radioactive isotopes.

| | $H$ (cm.) | | 4.5 | 5.5 | 10 | 100 |
|---|---|---|---|---|---|---|
| | $K^{40}$ | | $9.6\times10^{-3}$ | $9.0\times10^{-3}$ | $7.4\times10^{-3}$ | $2.1\times10^{-3}$ |
| Uranium-radium family | $Th^{234}$ | ($UX_1$) | $8.5\times10^{-5}$ | $6.5\times10^{-5}$ | $2.4\times10^{-5}$ | —— |
| | $Pa^{234}$ | ($UX_2$) | $1.76\times10^{-2}$ | $1.64\times10^{-2}$ | $1.41\times10^{-2}$ | $6.2\times10^{-3}$ |
| | $Pb^{214}$ | (RaB) | $2.8\times10^{-3}$ | $2.5\times10^{-3}$ | $1.9\times10^{-3}$ | $9.5\times10^{-5}$ |
| | $Bi^{214}$ | (RaC) | $2.30\times10^{-2}$ | $2.15\times10^{-2}$ | $1.85\times10^{-2}$ | $9.7\times10^{-3}$ |
| | $Bi^{210}$ | (RaE) | $7.6\times10^{-3}$ | $7.1\times10^{-3}$ | $5.8\times10^{-3}$ | $1.2\times10^{-3}$ |
| Uranium-actinium family | $Th^{231}$ | (UY) | $1.5\times10^{-4}$ | $8.3\times10^{-5}$ | $3.1\times10^{-5}$ | —— |
| | $Ac^{227}$ | (Ac) | $1.9\times10^{-4}$ | $1.6\times10^{-4}$ | $6.6\times10^{-5}$ | —— |
| | $Pb^{211}$ | (AcB) | $5.4\times10^{-3}$ | $5.0\times10^{-3}$ | $4.0\times10^{-3}$ | $5.7\times10^{-4}$ |
| | $Tl^{207}$ | (AcC″) | $1.00\times10^{-2}$ | $9.3\times10^{-3}$ | $7.9\times10^{-3}$ | $2.3\times10^{-3}$ |
| Thorium family | $Ac^{228}$ | ($MsTh_2$) | $1.05\times10^{-2}$ | $9.8\times10^{-3}$ | $8.3\times10^{-3}$ | $2.6\times10^{-3}$ |
| | $Pb^{212}$ | (ThB) | $7.8\times10^{-4}$ | $6.7\times10^{-4}$ | $4.3\times10^{-4}$ | —— |
| | $Bi^{212}$ | (ThC) | $1.72\times10^{-2}$ | $1.61\times10^{-2}$ | $1.38\times10^{-2}$ | $6.1\times10^{-3}$ |
| | $Tl^{208}$ | (ThC″) | $1.30\times10^{-2}$ | $1.21\times10^{-2}$ | $1.02\times10^{-2}$ | $3.8\times10^{-3}$ |

The counts per minute of beta-rays detected for any sample containing one per cent of potassium homogeneously, can be calculated according to equality (15), assigning $p_{K^{40}}=1.2\times10^{-6}$ and $N_{K^{40}}=2.41\times10^{5}$ and the values for $\frac{W}{C^*}G$ as in Table 4.

As for the counts regarding the uranium family, the calculation formula derived from equality (15) is as follows;

$$T_U=60\pi\left\{p_{U^{238}}N_{U^{238}}\sum_{UX_1,\cdots RaE}\left[\frac{W}{C^*}G\right]\right.$$
$$\left.+p_{U^{235}}N_{U^{235}}\sum_{UY,\cdots AcC'}\left[\frac{W}{C^*}G\right]\right\}, \qquad (32)$$

where $T_U$ denotes the counts per minute of beta-rays detected for any sample containing one per cent of natural uranium, and $p_{U^{238}}=0.00993$, $p_{U^{235}}=0.000071$, $N_{U^{238}}=1.24\times10^4$ and $N_{U^{235}}=8.0\times10^4$.

Similarly, the calculation formula for the counts regarding the thorium family is given by

$$T_{Th}=60\pi p_{Th}N_{Th}\left\{\left[\frac{W}{C^*}G\right]_{MsTh_2}+\left[\frac{W}{C^*}G\right]_{ThB}\right.$$
$$\left.+0.65\left[\frac{W}{C^*}G\right]_{ThC}+0.35\left[\frac{W}{C^*}G\right]_{ThC'}\right\}, \qquad (33)$$

where $p_{Th}=0.01$, $N_{Th}=4.13\times10^3$.

As a matter of course, in equalities (32) and (33) it is assumed that the radioactive equilibrium is held in the sample.

Numerical values thus obtained are tabulated in Table 5.

Table 5. Calculated counts per minute of beta-rays.

| $H$ (cm.) | 4.5 | | 5.5 | | 10 | 100 | |
|---|---|---|---|---|---|---|---|
| | $_{4.5}T$ | $_{4.5}T/_{10}T$ | $_{5.5}T$ | $_{5.5}T/_{10}T$ | $_{10}T$ | $_{100}T$ | $_{100}T/_{10}T$ |
| per 1% K | 0.52 | 1.29 | 0.49 | 1.21 | 0.404 | 0.116 | 0.29 |
| per 1% U | 1,200 | 1.26 | 1,110 | 1.17 | 950 | 450 | 0.47 |
| per 1% Th | 209 | 1.26 | 196 | 1.18 | 166 | 97 | 0.58 |

### *Test measurement*

Since it is difficult for measurement in the field to keep such strictly controled conditions as in the laboratory, and since we cannot eliminate the effect of gamma-rays, $T_m$, the number of counts per minute measured in the field somewhat differs from the calculated value of $T$. For a definite apparatus and a definite beta-active iso-

tope, the ratio of $T_m$ to $T$ may be considered as a constant $k$, that is

$$T_m = kT. \tag{34}$$

Hence, the ratio between $T_m$'s measured at different distance $H$, may be equal to the ratio between the relevant $T$'s calculated.

For the first example, measuring the radioactivity of chemical pure $K_2SO_4$ at $H$=0.8 cm., 1.0 cm., 4.5 cm. and 5.5 cm., we obtained the ratios as tabulated in Table 6. In the case at $H$=0.8 cm. and 1.0 cm., $x_1$ was 1.0 cm. and $\rho^*$=1.14, and the calculated value $T$ was obtained from Table 2 in the previous paper[1].

Table 6. Measured and calculated ratio between the counts for $K_2SO_4$ at different distances.

| | $_{0.8}T : _{1.0}T$ | $_{1.0}T : _{4.5}T$ | $_{4.5}T : _{5.5}T$ |
|---|---|---|---|
| Measured value | 1.21 | 0.94 | 1.04 |
| Calculated value | 1.24 | 1.03 | 1.07 |

Table 7. Measured and calculated ratios between the counts for a granite at different distances.

| | $_{5.5}T : _{10}T$ |
|---|---|
| Measured value | 1.15 |
| Calculated value | 1.17~1.21 |

For the second example, a ground granite block was measured at $H$=5.5 cm. and 10 cm.. At these distances the distribution of radio-active source in the granite may be regarded as homogeneous, so the calculation above described may be applied in this case as well. The results are shown in Table 7.

## *Discussion*

Throughout these measurements the apparatus used was Aloka DC-PI[3] made by the Electro-Medical Research Institute Ltd.. This apparatus was designed by the present author in order to measure the beta-radioactivity of ores and rocks in the field as precisely as possible, and to enable us to estimate the content of racioactive

isotopes in them. The calculations described in this paper are performed in order to give a foundation for that estimation. The validity of the calculation is confirmed by the results of measurement shown in Tables 6 and 7, allowing fhe error less than ten per cent.

Considering the roughness of the surface of ores and rocks as well as their heterogeneity, the author assignes the value of $H$ as 10 cm. for usual measurements. With this value of $H$, the radioactivity of the air between the sample and the counter is negligible in ordinary case but, in the field rich in radioactive minerals, especially in the gallery, it cannot be neglected. This problem will be discussed in another paper[2].

*Acknowledgement*

The writer wishes to express his gratitude to Professor T. Ito, Institute of Mineralogy, University of Tokyo, for critically reading the manuscript. Thanks are also due to the Geological Survey of Japan for furnishing the measuring apparatus, and to the Electro-Medical Research Institute Ltd. for collaborating with the writer in constructing the apparatus.

This investigation was aided by a grant from the Scientific Research Fund of the Department of the Education.

## References

1) Katayama, N.: Miner. Jour., 1, 170 (1954).
2) Katayama, N.: Sci. Pap. Coll. Gen. Ed. Univ. Tokyo, 5, No. 2 (1955).
3) Katayama, N.: to be published in Mining Geol., 6, (1956), in Japanese.

*Manuscript received August 20, 1955.*

MINERALOGICAL JOURNAL, VOL. 1, NO. 5, 313-322, DECEMBER, 1955

# DIELECTRIC BEHAVIOUR OF APOPHYLLITE AND ANALCITE*

RYÔITI KIRIYAMA, HIDEKO IBAMOTO, MITSUE KOIZUMI and RIKUSABURO KITAGAKI

*Department af Chemistry, Faculty of Science, Osaka University and Institute of Geological Sciences, North College, Osaka University*

ABSTRACT

The permittivity of apophyllite, $\varepsilon_C$, measured at room temperature was 6.4. This value is not so large as is usually expected for a hydrated crystal and, therefore, the atomic polarization effect of the hydrogen atom perpendicular to the O—H···O axis of the hydrogen bond is smaller than in crystals containing the hydrogen bond of the O—H ··O type. It is to be concluded that the water molecules in apophyllite are not tightly bound to the neighbouring oxygen atoms and are classified as normal water of crystallization. The temperature dependences of the dielectric constant were also studied.

The permittivity of analcite measured at 3 Mc. at room temperature was 6.5. A distinct dielectric dispersion was observed at room temperature in the audio-frequency region. From the observed data of $\varepsilon'$ and tan $\delta$, the energies and entropy of activation were obtained: $\Delta F^* = 12.7$ kcal/mole, $\Delta H^* = 14.5$ kcal/mole and $\Delta S^* = 4.8$ cal/deg. mole. It may be concluded that the water molecules in analcite are linked to the neighbouring oxygen atoms through the hydrogen bonds of energy of about 7.3 kcal/bond and are distributed over a set of equivalent positions in the structure. The dielectric dispersion observed in the temperature region between 200° and 500° C. seems to be attributable to the polarizing effect of dipole cluster formation similar to that found in $K_2HgCl_4 \cdot H_2O$.

## *Introduction*

There are a number of hydrated crystals which contain water molecules in definite proportions. The binding state of such water

* Read at the Annual Meeting of the Mineralogical Society of Japan, on June 5, 1954 and on June 4, 1955.

molecules will naturally be peculiar to each of the crystal structures and the accurate knowledge of the state may provides with some clues to the explanation of the growth conditions of these crystals. One of the effective ways of tuckling this important problem of crystallography and mineralogy is to accumulate and analyse the data of dipole orientation of water molecules, of their activation energies and of the entropy of dipole relaxation. From this standpoint, the authors have for some years been engaged in the study of the dielectric dispersion phenomena of some artificial crystals[2)3)4)5)7)]. The following article is to deal with the results of measurements recently carried out on water molecules in apophyllite and in analcite.

### *Apparatus and procedure*

The crystal condenser for the present dielectric measurements at room temperature was consisted of parallel plates and the capacity was determined by the resonance method at 3 Mc. stabilized with an appropriate quartz oscillator. The permittivities of crystals were obtained from the ratio of the capacities of tin-foiled specimens to that of artificial rock salt whose permittivity, 5.62, was taken as the standard.

For measurements in the audio-frequency region, a capacity-resistance bridge was used[6)]. The cell for measurements in high temperature regions was made of stainless steel and was placed in an electric furnace controlled with direct current from batteries. The condenser plates were covered tightly with platinum plates in order to avoid oxidation.

### *Permittivity of apophyllite*

The structure of apophyllite, $KFCa_4Si_8O_{20} \cdot 8H_2O$, is composed of $(Si_4O_{10})_\infty$-sheets extending parallel to the *c*-plane, interleaved with the sheets of the other constituent atoms, K, Ca, F and $H_2O$. According to the structure analysis,[11)] the water molecules in this structure are presumed to form hydroxyl bonds, HO-H-O, running parallel to

its $c$-plane. The crystal is, therefore, supposed to be an ideal material for discussing the dielectric polarization of the so-called hydroxyl bond.

The sample used in the present investigation was a well-developed crystal from the Kamioka Mine, Gifu Prefecture. The room temperature permittivity, $\varepsilon_c$, measured on a cleavage flake parallel to the basal plane was 6.4, the direction of the electric field thereby applied being parallel to the c-axis of the crystal. This value is comparable with the permittivities of normal ionic salts containing no hydrogen bond in their structures, such as 6.0 for sodium bromide, 8.4 for fluorite, 8.2 and 8.7 for calcite and is much less than the values

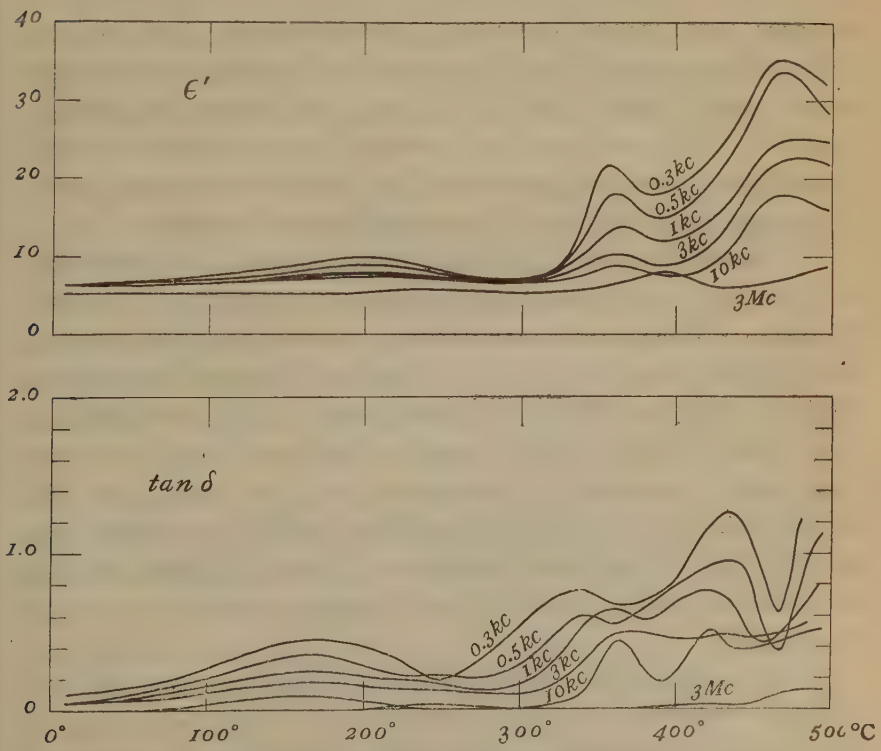


Fig.1. Temperature dependences of permittivity, $\varepsilon'_c$ ($\epsilon_c$), and dielectric loss, tan $\delta$, of apophyllite.

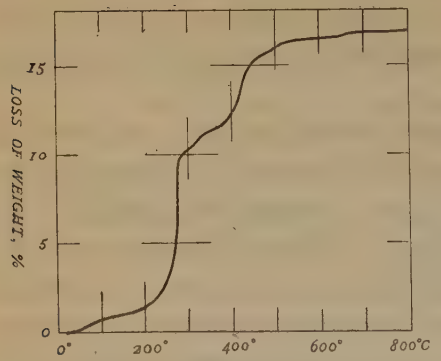


Fig. 2(a). Dehydration curve of apophyllite.

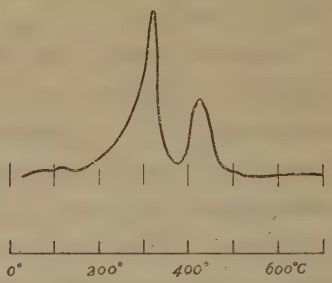


Fig. 2(b). Differential thermal analysis curve of apophyllite.

obtained with crystals containing hydrogen bonds. For example, the maximum permittivity of gypsum, the direction of which is almost perpendicular to the O-H-O bond axis, has been reported to be 10.6.[9] It is to be concluded, therefore, that the strength of the interaction of a water molecule to the neighbouring oxygen atom in the apophyllite structure is not so strong as in gypsum.

The temperature and frequency dependences of the dielectric constant and the loss factor were observed above 100° C. as shown in Fig. 1. These results are almost consistent with the thermal observations given in Fig. 2.[8] The small dielectric dispersion between 100°C. and 250°C. may be attributed to the dipole orientation of easily movable water molecules distributed presumably over some defect or random lattice points. On the other hand, the remarkable dispersions observed at about 350° C. and 450° C. are probably due to the dipole orientation of water molecules at the occasions of atomic rearrangements which take place at these temperatures.

It was impossible to measure the activation energies and the entropy of the hindered rotation of the water molecules owing to the lattice reconstruction and the partial dehydration occurred at these temperatures. It was also to be regretted that the specimen

for the measurement of $\epsilon_a$ could not be obtained because of the perfect basal cleavage of the crystal.

However, the authors believe that the following qualitative conclusion can be drawn from the experimental results described above; the water molecules in apophyllite are not so peculiar as have often been supposed but are classified as the water of crystallization of ordinary character and the molecules act as binding material attenuating the interaction between the calcium atoms and the phyllosilicate groups.

### *Permittivity of analcite*

Analcite, $NaAlSi_2O_6 \cdot H_2O$, is a typical zeolite and its structure was determined in 1930 by W. H. Taylor.[10] In this structure, water molecules are arranged in spiral tunnels running through the structure along the screw axes parallel to the three principal axes of the crystal.

The samples used in the present investigation were transparent crystal from Maze, Niigata Prefecture.* Specimens were prepared by grinding the crystals parallel to their natural (211) faces.

Since a considerable dielectric dispersion was observed at room temperature, measurements were also made at low temperatures and in higher frequency regions in oder to obtain the value of permittivity free from orientation polarization. The results obtained at −50° C. were 6.6 at 10 kc., 7.0 at 1 kc. and 7.2 at 0.3 kc., and at room temperature, 6.5 at 3 Mc.. The value at 3Mc. at room temperature coincides with those at 10 kc. and at 5 kc., both at −50° C., within the experimental error. Hence the value of the permittivity free from orientation polarization was determined to be 6.5.

During the course of the experiment, a distinct dielectric dispersion of the Debye type appeared between 0° and 200° C. in the

* The authors wish to thank Prof. N. Katayama and Dr. K. Sakurai for placing several samples of analcite under their disposal.

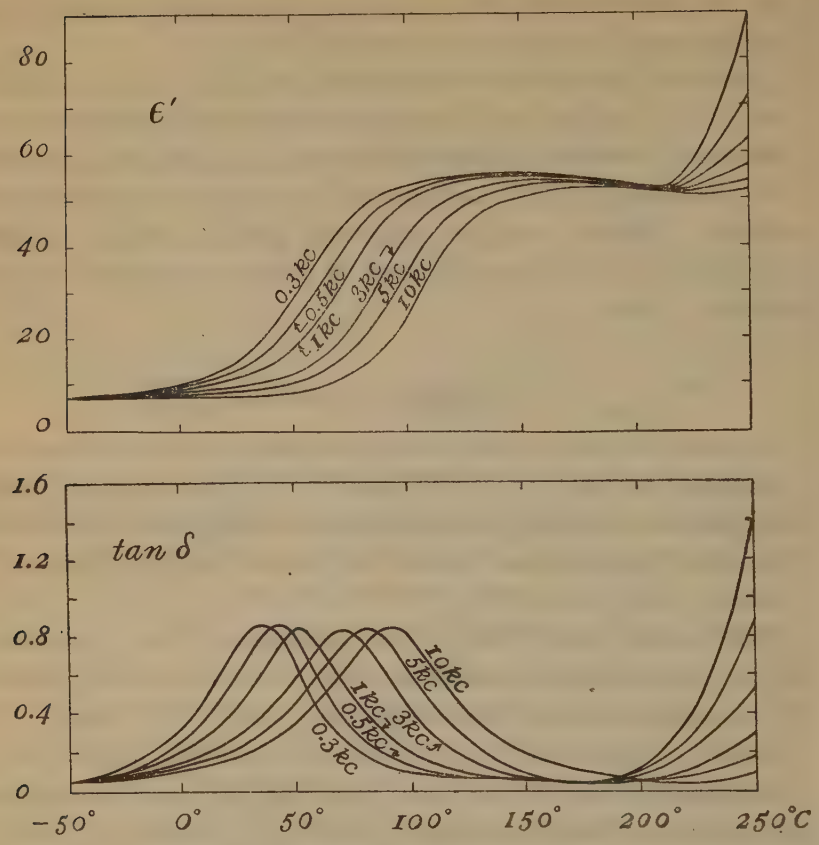


Fig. 3. Temperature dependences of permittivity, $\epsilon'$ ($\epsilon$), and dielectric loss, tan $\delta$, of analcite.

audio-frequency region as is seen in Fig. 3. Another dispersion was also observed at a higher temperature. Fortunately, as there was no overlapping of these dispersion maxima in the tan$\delta$-$T$ diagram, these could be considered separately with reference to the results of thermal observations.

Then, $\epsilon''$-values were calculated from the observed tan $\delta$ and $\epsilon'$ at various frequencies and were plotted in the Cole-Cole diagram (Fig. 4). It was found that these points in the diagram were aligned in

an arc of a circle whose centre was located slightly below the abscissa, *i. e.* ε′-axis. It was, therefore, concluded that the orientation process was accompanied by a small distribution of relaxation

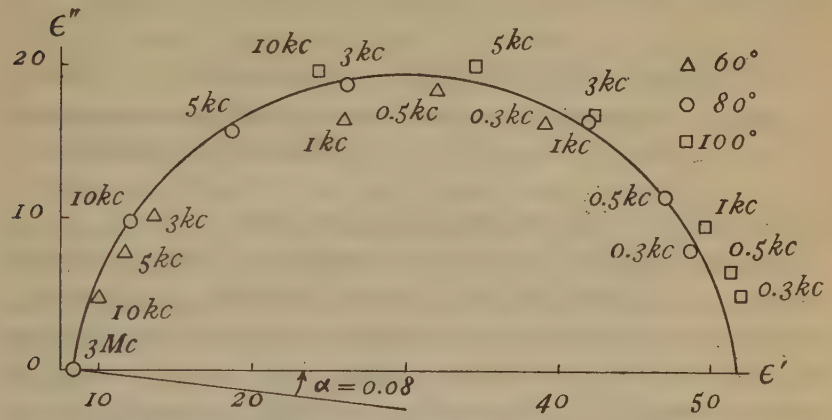


Fig. 4. Cole-Cole diagram of analcite at 60°, 80° and 100°C. The semicircle shows the frequency dependences at 80°C.

time ($\alpha$=0.08). A single relaxation being assumed, the energies and entropy of activation were derived from the Debye-Eyring relations as follows:

free energy of activation $\Delta F^*$=12.7 kcal/mole,

enthalpy of activation $\Delta H^*$=14.5 kcal/mole,

entropy of activation $\Delta S^*$=4.8 cal/deg. mole at 450° K.

In order to confirm the validity of the conclusion mentioned above experiments on the thermal analysis of the crystal were also carried out and the dehydration curve as shown in Fig. 5 (a)[8] was produced. As there was no noticeable loss of weight observed below 200° C., it was established that the dielectric relaxation phenomenon occurred below 200° C. was due only to the dipole orientation of the water molecules and not to the surface conduction effect caused by escaping water molecules from the crystal lattice. As to the slight rise of the differential thermal analysis curve below 200° C. (Fig. 5 (b)[8], the authors suppose that it was caused by some thermal

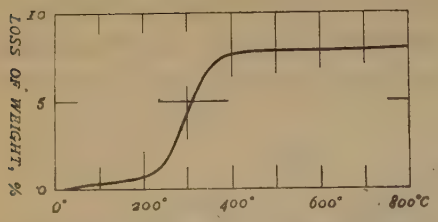


Fig. 5(a). Dehydration curve of analcite.

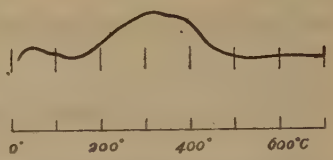


Fig. 5(b). Differential thermal analysis curve of analcite.

motions of the water molecules within the lattice.

From the results of the dielectric measurements and the thermal analyses so far described, the following suggestion may be given; the water molecules enclosed in the holes in the structure of analcite are bound to the neighbouring oxygen atoms, each of which is shared by two (Si, Al) $O_4$-tetrahedra, through hydrogen bonds of about 7.3 kcal/bond (a half of the value of the enthalpy of activation, 14.5 kcal/mole) and easily begin to orientate themselves according to the applied electric field, even at room temperature in a low frequency region.

The positions of the water molecules in the analcite structure have not fully been confirmed by X-ray evidences but merely been assumed from the symmetry of the crystal as well as from the zeolitic nature of the crystal. However, the fact that $\alpha$ derived from the Cole-Cole diagram is considerably small seems to suggest that the dielectric dispersion should be attributed to a single relaxation mechanism and, therefore, every water molecule in the unit cell is in the same binding state. This suggestion from the dielectric study of the crystal is in agreement with what was presumed on the structure analysis; the water molecules would be distributed over a set of equivalent points in the structure.

Next stage of the investigation is to deal with the dielectric dispersion observed above 200°C.. This will also be due to the orientation polarization of the water molecules but it must contain the effect

of surface conduction caused by dehydrated water molecules. In fact, the specimen, after having been heated up to about 300° C. in the cell of the dielectric measurements showed a appreciable weight loss and became white and translucent. Since it is quite certain that dehydration had taken place, it is impossible to deal with the case under consideration as quantitatively as we did with that in the lower temperature region, but the following factors may be conceived of as responsible to the occurrence of a high dielectric constant observed in the region now being described: 1) dipole orientation of the water molecules in the structure, 2) formation of dipole clusters in the tunnels in the structure at the stage of pre-dehydration just as the case of the behaviour of water molecules in $K_2HgCl_4 \cdot H_2O$[7] and 3) conduction effect caused by water molecules adsorbed either on the surface of the crystal or in cracks in it. Judging from the experimental results obtained with $K_2HgCl_4 \cdot H_2O$[7] and gypsum,[3] however, the authors concluded that the second factor would contribute most to the high dielectric constant of the crystal. Namely, in the course of experiments on partially dehydrated gypsum, no distinct rise of the dielectric constant is observed during its gradual dehydration, and together with this fact, the detailed surface-chemical study of gypsum and the confirmed zeolitic nature of the hemihydrate[1] seem to eliminate the first factor. The third factor can also be neglected because both for $K_2HgCl_4 \cdot H_2O$ and for gypsum, monotonous decrease of their dielectric constant can be observed about 120°~130° C. in spite of their gradual dehydration in this temperature range. Thus, the second factor will be the one which makes predominant contribution to the occurrence of the high dielectric constant in analcite.

Then, the authors studied the anisotropy of the dielectric polarization of analcite. The structure of $K_2HgCl_4 \cdot H_2O$ has tunnels parallel to its c-axis and accordingly, its high dielectric polarization appears only in this direction. Whereas, in the structure of analcite, spiral tunnels are formed in three directions parallel to its four-fold axes

and, therefore, the large polarization is expected to be observed in any direction in accordance with the isometric nature of the crystal. This was cosfirmed by measuring the dielectric polarization of the specimen along its arbitrary direction.

As the temperature becomes higher, the thermal motion of the water molecules will correspondingly be stronger and the chances of cluster formation will decrease. The dielectric polarization will, therefore, diminish as is actually seen in the values of permittivity at low frequencies between 450° and 550° C.. The details of these data differ from specimen to specimen, but the general tendency is always maintained.

In conclusion, the dielectric behaviour of water molecules in analcite shows a distinct low frequency dispersion of the Debye type in the neighbourhood of or above room temperature. This indicates that the water molecules in the mineral are linked to the nearest oxygen atoms of the silicate framework through the hydrogen bonds of energy of about 7 kcal/bond. Thus, it will be quite understandable that the so-called zeolitic water, though so easily removable from the structure, plays an important role in stabilizing the structure at its growth stage.

## References

1) Gregg, S. J. and E. G. J. Willing: J. Chem. Soc. London, 1951, 2373; 2916.
2) Kiriyama, R. and H. Ibamoto: Bull. Chem. Soc. Japan, 25, 359 (1952).
3) Kiriyama, R. and H. Ibamoto: *ibid.*, 26, 109 (1953).
4) Kiriyama, R. and Y. Saito: *ibid.*, 26, 531 (1953).
5) Kiriyama, R. and H. Ibamoto: *ibid.*, 27, 32 (1954).
6) Kiriyama, R., S. Yabumoto and I. Nitta: *ibid.*, 27, 115 (1954).
7) Kiriyama, R. and H. Ibamoto: *ibid.*, 27, 317 (1954).
8) Koizumi, M.: Miner. Jour., 1, 36 (1953).
9) Narayana Rao, D. A. A. S.: Proc. Ind. Acad. Sci., 27A, 177 (1948).
10) Taylor, W. H.: Z. Krist., 74, 1 (1930).
11) Taylor, W. H. and St. Nàray-Szabò: Z. Krist., 77, 146 (1931).

*Manuscript received August 22, 1955.*

MINERALOGICAL JOURNAL, VOL. 1, NO. 5, PP. 323-327 DECEMBER, 1955

## SHORT COMMUNICATIONS

# BOULANGERITE IN SULPHIDE ORES FROM THE OBIRA MINE, KYUSHU, JAPAN

MICHITOSHI MIYAHISA

*Institute of Economic Geology, Faculty of Engineering, Kyushu University*

### *Introduction*

In the course of study of mineralization on the Obira tin deposit, the writer found boulangerite [$Pb_5$ $Sb_4$ $S_{11}$] among the other lead antimony iron sulphide minerals (jamesonite and berthierite, etc.).

Two localities of boulangerite have alreadp been reported in Japan, the Toroku Mine, Miyazaki Prefecture,[1] and the Yoshiwara Mine, Fukuoka Prefecture.[2] In this paper the writer gives some descriptions of the boulangerite from the new locality, and his considerations on the genetical relation between the pre-existing galena and the later antimony-bearing ore solutions.

### *An Outline of the ore deposit*

The Obira Mine, Ogata-machi, Ono-gun, Oita Prefecture, is situated at about 30 km. south of the Ogata station of Hohi Line. It was worked for tin, zinc, lead, copper and arsenic for long years.

The surrounding district of the mine is geologically composed of the Paleozoic group, the sheared granites of early Mesozoic, the Mitate conglomerate probably of early Tertiary, the Sobosan volcanic rocks, and the younger acid intrusive complex. The ore deposits are genetically related to the acid intrusives that is, granitic rocks of Miocene epoch, and can be classified as follows;

(1) Contact metasomatic deposits (zinc and lead bearing garnet-

hedenbergite-axinite-datolite-lievrite skarn masses.

(2) Pneumatolytic ~ hydrothermal tourmaline-fluorite-cassiterite-quartz veins.

(3) Hypothermal~epithermal sulphide veins, in which boulangerite was discovered.

### *Mode of occurrence*

The Boulangerite is found in the antimony ores in the Dohi-myaku (copper arsenic vein). It is commonly accompanied with galena, the latter being usually bordered or cut by the former. In some cases, boulangerite penetrates into pre-existing minerals such as quartz, pyrrhotite and chalcopyrite. It occurs abundantly as fine granular aggregates, or as felted aggregates of small acicular crystals.

### *Ore-microscopic observations*

Under the ore-microscope, the boulangerite shows the following characters.

Polishing: a good polish.

Reflection colour: white, with somewhat bluish green tint compared with galena, and the discrimination of colour is more distinct in oil than in air.

Reflection pleochroism: distinct, especially in oil immersion; parallel to elongation, white; perpendicular to elongation, greenish grey white.

Anisotropism under the crossed nicols: strong, with polarization colours; dark grey, brown, blue or greenish grey.

Hardness: the same as galena, Talmage B.

Etch tests: $HNO_3$ (1:1), stains black; HCl (1:1), KOH, $FeCl_3$ KCN, and $HgCl_2$, negative.

Form and texture (Plate I, Figs 1, 2 and 3): fibrous, needle-shaped or acicular; up to 0.1 mm. long; cleavage or twinning, not observed; replaces galena, and sometimes includes various fine minerals such as chalcopyrite, stannite, sphalerite, and pyrrhotite.

Microchemical tests: the lead iodide test and double iodide test[3] indicate that Pb, Sb and S are the major constituents of this mineral; tests for Sn, Fe, Ag and As, negative.

Teble 1. X-ray powder data for boulangerite. 1 and 2, copper radiation, camera diameter 28.8 mm.. 3, after S. C. Robinson[4], copper radiation.

| 1 | | 2 | | 3 | |
|---|---|---|---|---|---|
| Obira Mine | | Bohemia | | Sullivan Mine, Br. Columbia | |
| *I* | *d* (Å) | *I* | *d* (Å) | *I* | *d* (Å) |
| | | | | ½ | 6.74 |
| | | | | 1 | 6.13 |
| | | | | ½ | 5.20 |
| | | | | ½ | 4.86 |
| | | | | ½ | 4.61 |
| | | | | 1 | 4.36 |
| 3 | 3.92 | 2 | 3.95 | 2 | 3.89 |
| 10 | 3.73 | 10 | 3.72 | 10 | 3.71 |
| 2 | 3.40 | 4 | 3.45 | 1 | 3.43 |
| 2 | 3.28 | | | 3 | 3.32 |
| 3 | 3.19 | 3 | 3.23 | 5 | 3.21 |
| 8 | 2.99 | 8 | 2.94 | 4 | 3.02 |
| 10 | 2.80 | 10 | 2.81 | 8 | 2.815 |
| 1 | 2.69 | 2 | 2.69 | 3 | 2.691 |
| | | 1 | 2.54 | 1 | 2.578 |
| | | | | ½ | 2.515 |
| | | | | 1 | 2.435 |
| 5 | 2.34 | 4 | 2.36 | 5 | 2.337 |
| | | | | ½ | 2.303 |
| 1 | 2.18 | 1 | 2.24 | ½ | 2.226 |
| 4 | 2.144 | 2 | 2.169 | 4 | 2.145 |
| 1 | 2.026 | 1 | 2.093 | 2 | 2.056 |
| 5 | 2.005 | 1 | 2.012 | 1 | 1.967 |
| 2 | 1.918 | 2 | 1.931 | 2 | 1.920 |
| 8 | 1.854 | 7 | 1.862 | 7 | 1.861 |
| | | 1 | 1.794 | ½ | 1.829 |
| 7 | 1.761 | 5 | 1.765 | 6 | 1.757 |
| 1 | 1.725 | 1 | 1.725 | 2 | 1.726 |
| 1 | 1.662 | | | 1 | 1.668 |
| 1 | 1.637 | | | 2 | 1.657 |
| 2 | 1.586 | | | ½ | 1.588 |
| 2 | 1.534 | | | ½ | 1.537 |
| | | | | 1 | 1.504 |
| 2 | 1.464 | | | 1 | 1.465 |
| 4 | 1.409 | 3 | 1.409 | 2 | 1.408 |
| | | | | 1 | 1.378 |
| 5 | 1.323 | 4 | 1.324 | | |
| | | | | ½ | 1.303 |
| 2 | 1.234 | 3 | 1.243 | 1 | 1.239 |
| | | 4 | 1.216 | | |

### *X-ray examination*

The results of measurements of X-ray powder photograph of the boulangerite from the Obira mine is listed in Table 1. It is identical with those of the boulangerites from Bohemia and the Sullivan mine.

### *Genesis*

The Obira tin deposits are of telescoped type. There are two champion veins called Honpi and Dohi-myaku, in which several successive mineralizations have been recognized[4] as follows;

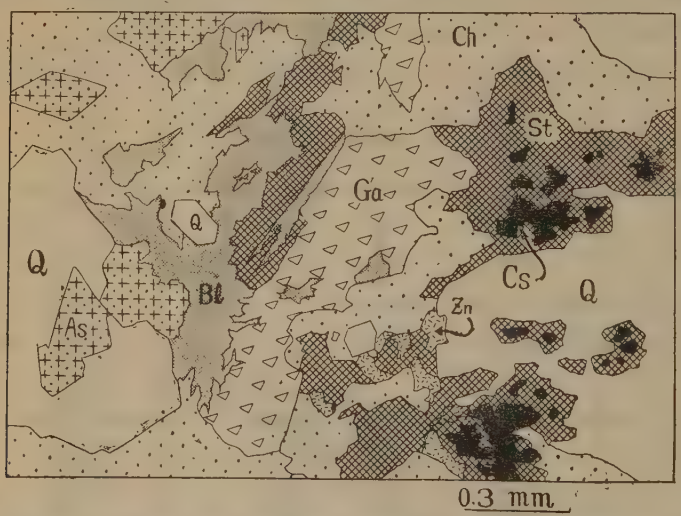


Fig. 4. Sketch showing the paragenetic relation of cassiterite (Cs), arsenopyrite (As), quartz (Q), chalcopyrite (Ch), stannite (St), sphalerite (Zn), galena (Ga), and boulangerite (Bl).

(1) deposition of cassiterite, quartz, apatite and tourmaline,

(2) deposition of cassiterite (large quantity), quartz, wolframite, molybdenite and pyrite,

(3) deposition of quartz, pyrite and arsenopyrite,

(4) deposition of sphalerite (marmatite), chalcopyrite, cubanite,

valleriite, pyrrhotite, stannite, native bismuth, bismuthinite and galena,

(5) deposition of marcasite (germanium-bearing) and quartz, and

(6) deposition of stibnite, berthierite, jamesonite, boulangerite, quartz, and carbonate minerals,

The Boulangerite and the other antimony sulphide or sulphosalt minerals were the last products of the hypogen metallization. At the time of the last antimony mineralization, the galena and some of the other simple sulphide minerals were not stable against the newly introduced ore-solution. Consequently, they were attacked by it and kinds of new sulphosalts minerals were formed. The paragenetic texture of the boulangerite and the galena suggests that lead in the boulangerite derived from the galena.

In the same manner, the breakdown of simple iron sulphide minerals led to the formation of berthierite [$FeSb_2S_4$] or jamesonite [$Pb_4FeSb_6S_{14}$].

*Acknowledgements*

The writer wishes to express his thanks to Prof. K. Kinoshita of Kyushu University for his kind guidance and criticism, and to Dr. K. Sakurai for providing the sample of boulangerite from Bohemia used in this study. Thanks are also due to the staff of the Obira mine, especially to Messrs. K. Watanabe and M. Maki who assisted the writer in the field work.

The study was supported in part by a grant from the Scientific Research Fund of the Educational Department in 1954.

## REFERENCES

1) Ito, T. & K. Sakurai: Wada's Minerals of Japan, 3rd Ed., vol. 1, 121 (1947) (in Japanese).
2) Sakurai, K.: Chigaku-Kenkyu, 6, 210 (1952) (in Japanese).
3) Short, M. S.: U. S. Geol. Surv. Bull., 914, 214 (1940).
4) Robinson, S. C.: Amer. Mineral., 33, 716 (1948).
5) Miyahisa, M.: Jour. Mining Inst. Kyushu, 22, (1954) (in Japanese).

*Manuscript received May 12, 1955.*

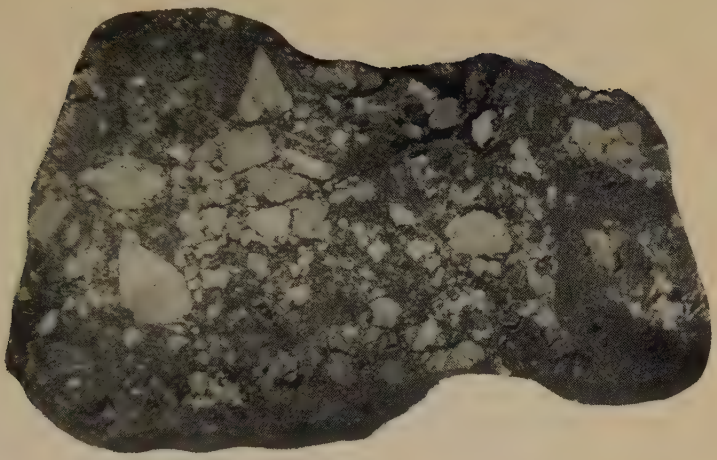

Fig. 1

2 cm

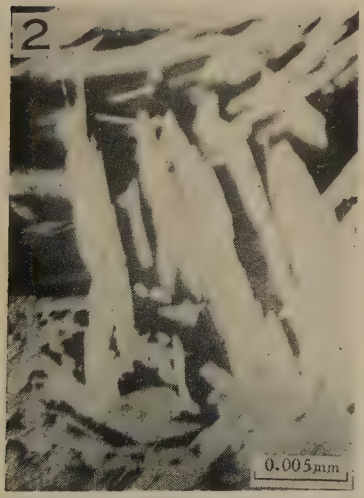


Fig. 2

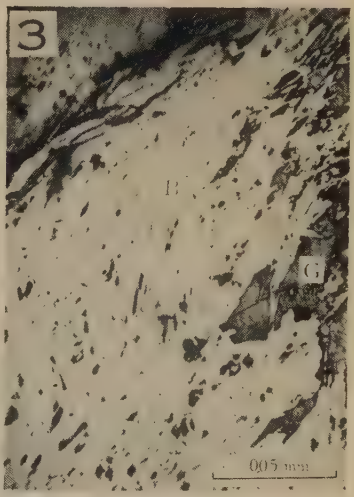


Fig. 3

Fig. 1. Polished surface of brecciated ore, showing relation of earlier sulphides (breccia) to later antimony minerals (matrix).

Fig. 2. Photomicrograph showing acicular or fibrous aggregates of boulangerite, oil immersion. Polarizer only.

Fig. 3. Photomicrograph showing the boulangerite (B) which replaces galena (G). Etched with HCl (1:1). Polarizer only.

MINERALOGICAL JOURNAL VOL, 1, NO. 5, PP. 329-336, DECEMBER, 1955

# A NEW METHOD FOR ESTIMATING THE TERMINATION EFFECT IN FOURIER ANALYSIS

KENZI DOI

*Mineralogical Institute, University of Tokyo*

The electron density in a crystal is to be computed as a Fourier transform in reciprocal space. For the special purpose of estimating the termination effect, the writer has introduced the following device. First of all the observed reciprocal space should be divided into several shells as represented in Fig. 1. Starting from the transform of the innermost shell, and adding to it those of following shells succesively, we can obtain the usual values of electron densities $\rho\ (xy)$. In the course of this procedure $\rho_n\ (xy)$, the Fourier transform of innermost $n$ shells in the observed reciprocal space, makes variations with increasing numbers of contributing shells $n$, as shown typically in Figs. 2, 3-a, and 4-a, where the ordinates mean values of $\rho_n\ (xy)$ and the abscissae the values of $n$.

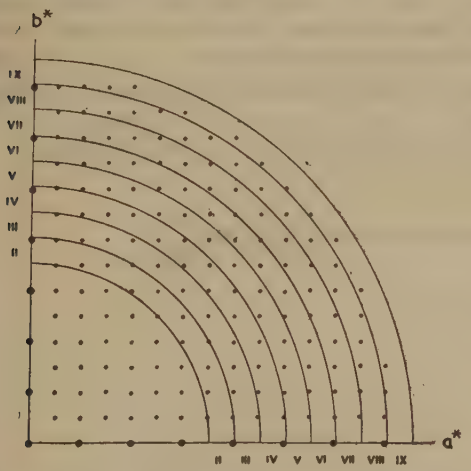


Fig. 1. The observed reciprocal space of salicylic acid crystal. Shell numbers correspond to those in Figs. 2, 3, and 4.

In Fig. 2, the usually obtained value of $\rho\ (xy)$ is read from point A. When we draw, however, the upper and lower envelopes aA and bB, it will be recognised that the most probable value of electron

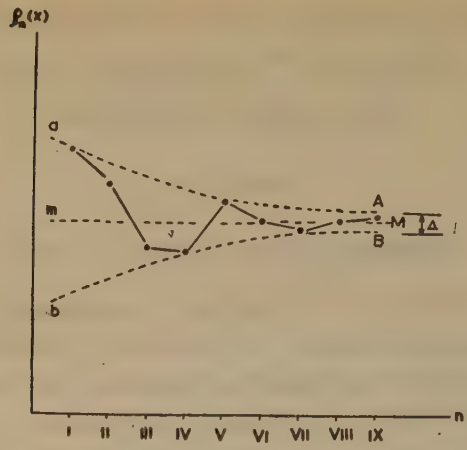


Fig. 2. First type of variation. Solid circles and segments represent the variation of $\rho_n(xy)$ with respect to $n$, for $x=15/60$, $y=9/60$. Dotted curves aA and bB are the upper and lower envelopes, and mM is the median line of these envelopes. The ordinate of M gives the values of $\rho_\infty(xy)$, the difference between the ordinates of A and B measures the termination effects.

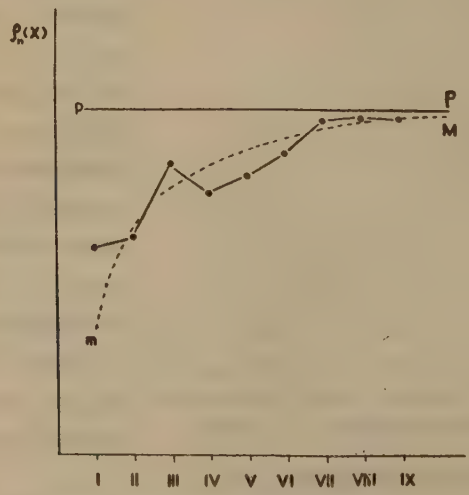


Fig. 3 (a). Second type of variation. Solid circles and segments represent the variation of $\rho_n(xy)$ for $x=4/60$, $y=22/60$. Dotted curve mM is exponential median curve, pP its asymptote. $\rho_\infty(xy)$ is read from the ordinate of P.

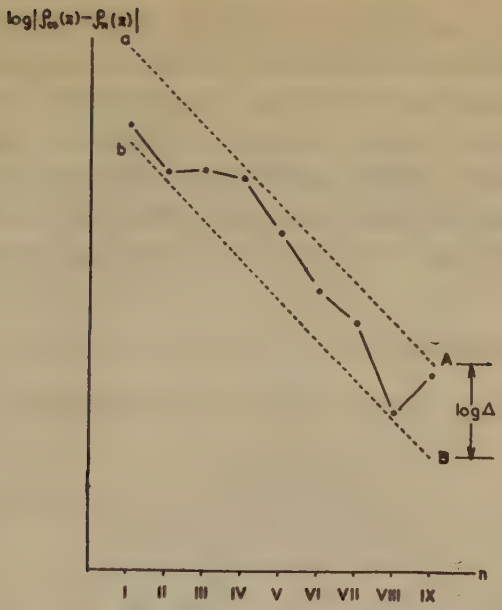


Fig. 3 (b). Soild circles and segments represent the variation of log $|\rho_\infty(xy) - \rho_n(xy)|$ for the same $x$- and $y$- coordinates as in Fig 3 (a). Dotted parallel lines aA and bB are upper and lower envelopes. The difference of ordinates of A and B measures the logarithm of termination effects at this point.

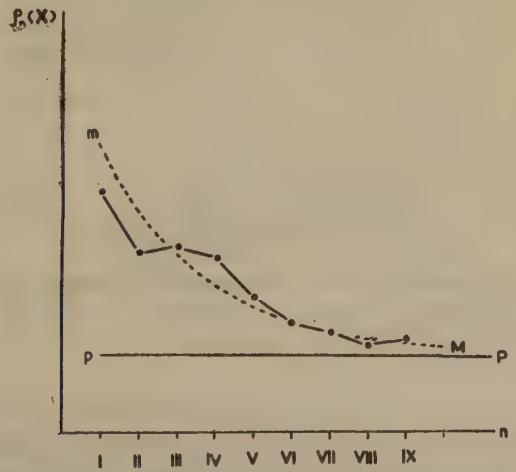


Fig. 4(a). Third type of variation. Soild circles and segments represent the variation of $\rho_\infty(xy)$ for $x=1/60$, $y=21/60$. Dotted curve mM is the exponential median curve, and pP its asymptote. $\rho_\infty(xy)$ is read from the cordinate of P.

density $\rho_\infty(xy)$, is not likely to be A, but to be M, the median point of A and B. The error associated can be estimated to be $\Delta=\overline{AB}$.

When the variation is like that as represented in Fig. 3-a or Fig. 4-a, it will be generally possible to assume by inspection the exponential median curve mM and its asymptote pP. The most probable electron density $\rho_\infty(xy)$, may be read at P, and the termination error associated to be $\log \Delta=\overline{AB}$ in Fig. 3-b or Fig. 4-b, where

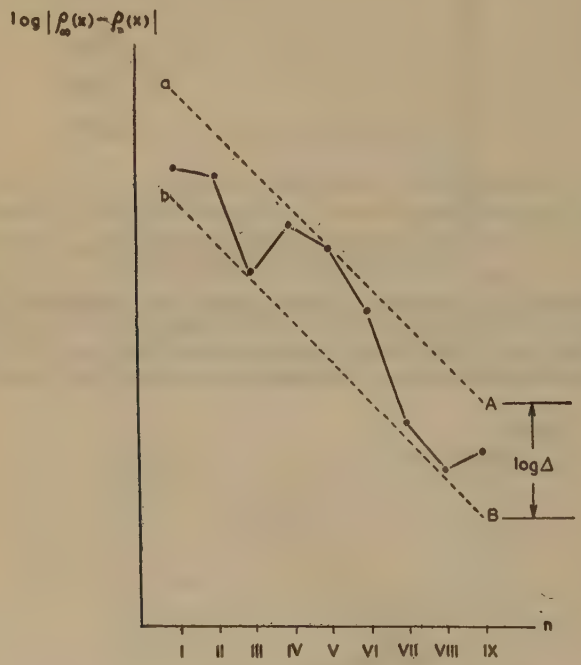


Fig. 4 (b). Soild circles and segments represent the variation of $\log|\rho_\infty(xy)-\rho_n(xy)|$ for the same $x-$ and $y-$ coordinates as in Fig. 4(a). Dotted lines aA and bB are upper and lower envelopes.

the ordinates mean $\log|\rho_\infty(xy)-\rho_n(xy)|$ (the median curve mM being drawn so that aA and bB in Fig. 3-b or Fig. 4-b should be parallel straight lines).

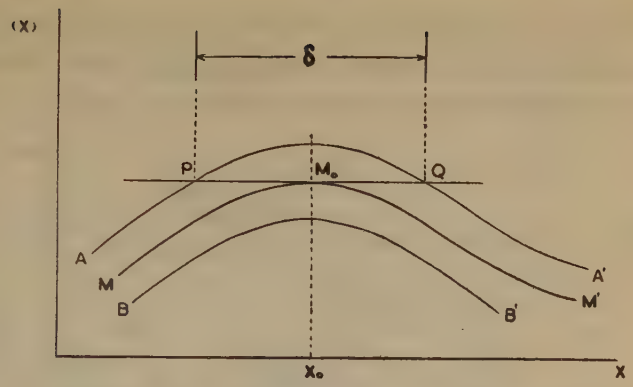


Fig. 5. Termination effect on atomic coordinate. See the text.

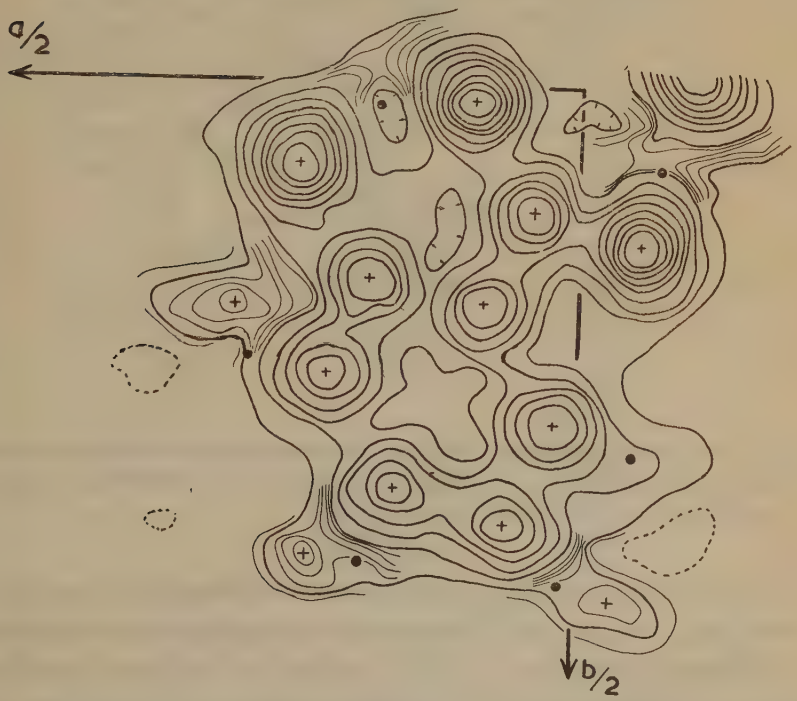


Fig. 6. The most probable electron density $\rho_{\infty}(xy)$ in the salicylic acid crystal. Thick contours are at every 1 e/Å$^2$, thin ones at every 0.2 e/Å$^2$, zero levels broken. Crosses show the present writer's determination of atomic positions, small black circles show the positions of hydrogen atoms determined by Cochran.

By means of the procedures described above, we can derive the most probable values of electron densities and the probable termination errors associated for every point in the unit cell.

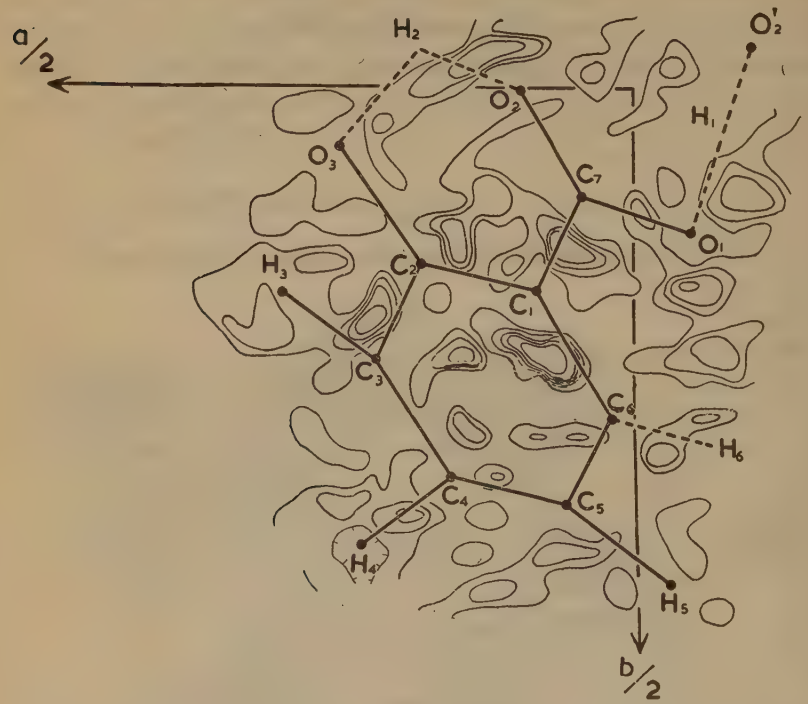


Fig. 7. Probable termination errors $\Delta(xy)$ superposed with the skeleton of molecule. Contours are at every 0.1 e/Å2. Small black circles show the atomic positions determined by the present writer.

The most probable atomic coordinates are determined as maximum points in $\rho_\infty(xy)$, the termination errors of which are estimated with the following procedures. In Fig. 5 let MM' be the most probable electron density curve, AA' and BB' the upper and lower limits of termination errors associated to MM'. The most probable atomic coordinate should be the coordinate of the maximum point of curve MM', say $x_0$, and the errors associated with $x_0$ will be $\delta=\overline{FQ}$, where

Table 1. The atomic coordinates in salicylic acid crystal.

| Atoms | | Present writer | Cochran |
|---|---|---|---|
| O(1) | $x$ | 0.050±0.002 | 0.0514 |
| | $y$ | 0.137±0.002 | 0.1370 |
| O(2) | $x$ | 0.100±0.002 | 0.0990 |
| | $y$ | 0.017±0.002 | 0.0164 |
| O(3) | $x$ | 0.250±0.001 | 0.2503 |
| | $y$ | 0.074±0.001 | 0.0705 |
| C(1) | $x$ | 0.083±0.003 | 0.0841 |
| | $y$ | 0.192±0.008 | 0.1926 |
| C(2) | $x$ | 0.183±0.005 | 0.1848 |
| | $y$ | 0.168±0.005 | 0.1697 |
| C(3) | $x$ | 0.218±0.003 | 0.2207 |
| | $y$ | 0.252±0.003 | 0.2512 |
| C(4) | $x$ | 0.158±0.005 | 0.1570 |
| | $y$ | 0.350±0.001 | 0.3520 |
| C(5) | $x$ | 0.058±0.004 | 0.0576 |
| | $y$ | 0.375±0.003 | 0.3755 |
| C(6) | $x$ | 0.025±0.005 | 0.0208 |
| | $y$ | 0.295±0.005 | 0.2977 |
| C(7) | $x$ | 0.043±0.005 | 0.0456 |
| | $y$ | 0.108±0.005 | 0.1097 |
| H(3) | $x$ | 0.30 ±0.03 | 0.286 |
| | $y$ | 0.19 ±0.01 | 0.233 |
| H(4) | $x$ | 0.233±0.008 | 0.188 |
| | $y$ | 0.408±0.004 | 0.399 |
| H(5) | $x$ | 0.03 ±0.05 | 0.017 |
| | $y$ | 0.46 ±0.03 | 0.431 |

Table 2. Values of carbon-hydrogen distances.

| | Doi | Cochran |
|---|---|---|
| C(3)-H(3) | 1.06±0.3 Å | 0.90 Å |
| C(4)-H(4) | 1.13±0.07 | 0.90 |
| C(5)-H(5) | 1.15±0.4 | 0.78 |

P and Q are intersections between the tangent of MM′ at the atomic position $M_o$ and the curve AA′.

The above procedures were applied for the (*hk*0) reflections of salicylic acid observed by W. Cochran[1]. The most probable electron densities obtained are represented in Fig. 6 and the termination errors associated, in Fig. 7. In Fig. 6 we can clearly notice weak peaks in the vicinity of carbon atoms, which are, though very weak, not submerged under the termination errors, and may be attributed to hydrogen atoms attached to the benzene ring. For the hydrogen atoms $H_1$, $H_2$, and $H_6$, no isolated peaks were obtained by the present procedures. The atomic coordinates with their termination errors read from Figs. 6 and 7 are listed in Table 1 along with those obtained by Cochran by means of difference Fourier synthesis. Newly determined C-H distances are listed in Table 2 together with those of Cochran's. In determining these distances the writer assumed the same *z*-coordinates as given by Cochran.

## Reference

1) Cochran, W.: Acta cryst., **6**, 260 (1953).

*Manuscript received September 1, 1955*

# Contents of "KOBUTSUGAKU ZASSHI,"

## Journal of the Mineralogical Society of Japan

*in Japanese*

---

VOL. 2, No. 4 (September, 1955)

*Addresses*

On the Manganese Deposits of India and Their Minerals ..... T. Watanabe ...233

*Original Articles*

On the Dielectric Behaviour and the X-Ray Investigation of Some Metamict Minerals.....Y. Ukai, M. Korekawa and Y. Mochida...252

On Amblygonite from Nagatare-yama, Fukuoka Prefecture.....J. Ito, H. Minato and Y. Okamoto...263

Chemical Compositions of the Mineral Belonging to Euxenite-Polyclase Series from the Nekonaki Pegmatites in Ishikawa Town, Fukushima Prefecture.....K. Omori and S. Hasegawa...268

Pisolitic Limonite from the Matsuiwa Mine, Miyagi Prefecture.....M. Nambu...275

*Short Communications*

Druse Hypersthene from Iki Island .....I. Sunagawa, T. Hayashi and K. Matsui...282

Clay Minerals around Hot Springs.....H. Minato...287

Limonite in Oniita (Demon-Plate) from Seto, Aichi Prefecture..... K. Hukuo...292

*Reviews*

Hydrothermal Reaction of Minerals..... R. Kiriyama and M. Koizumi...297

*Proceedings* .....316

*Printed by "HERALD" Printing Co., Ltd.*